Ultrafast Science
A SCIENCE PARTNER JOURNAL

REVIEW ARTICLE

Review and Prospect of Single-Shot Ultrafast Optical Imaging by Active Detection

Xuanke Zeng†, Xiaowei Lu†, Congying Wang, Kaipeng Wu, Yi Cai*, Hongmei Zhong, Qinggang Lin, Jiahe Lin, Ruiwei Ye, and Shixiang Xu*

Key Laboratory of Optoelectronic Devices and Systems of Ministry of Education and Guangdong Province, Shenzhen Key Lab of Micro-Nano Photonic Information Technology, College of Physics and Optoelectronic Engineering, Shenzhen University, Guangdong 518060, China.

*Address correspondence to: shxxu@szu.edu.cn (S.X.); caiyi@szu.edu.cn (Y.C.)
†The authors contributed equally to this work.

Citation: Zeng X, Lu X, Wang C, Wu K, Cai Y, Zhong H, Lin Q, Lin J, Ye R, Xu S. Review and Prospect of Single-Shot Ultrafast Optical Imaging by Active Detection. *Ultrafast Sci.* 2023;3:Article 0020. https://doi.org/10.34133/ultrafastscience.0020

Submitted 1 February 2023
Accepted 24 March 2023
Published 12 April 2023

In the recent decade, single-shot ultrafast optical imaging by active detection, called single-shot active ultrafast optical imaging (SS-AUOI) here, has made great progress, e.g., with a temporal resolution of 50 fs and a frame rate beyond 10 trillion frames per second. Now, it has become indispensable for charactering the nonrepeatable and difficult-to-reproduce events and revealing the underlying physical, chemical, and biological mechanisms. On the basis of this delightful status, we would like to make a review of SS-AUOI. On the basis of a brief introduction of SS-AUOI, our review starts with discussing its characteristics and then focuses on the survey and prospect of SS-AUOI technology.

Introduction

It is extremely important to discover and reveal ultrafast dynamic events, e.g., interactions of laser pulses and materials [1], fast ignition for laser inertial-confinement fusion [2], shock waves in living cells [3], valence electron dynamics in chemical reactions [4], and excitonic dynamics in photosynthetic light harvesting [5]. Ultrafast optical imaging, as a powerful method to realize blur-free visualization of transient dynamics, has gotten great interest for decades in many fields, from physics [6–8], chemistry [4,9–11], and materials science [12] to industrial processing and manufacturing [13–16] and biomedicine engineering [17–19]. Some of transient events are well reproducible with high repetition rates and, thus, can be well recorded by the time-resolved pump–probe imaging [20,21]. However, some others occur without repeatability or with bad repeatability, e.g., optical rogue waves [22], irreversible phase transitions [23], and ultraintense laser–plasma interactions [24]. For this kind of targets, the pump–probe methods become not to be feasible; instead, some single-shot techniques are required.

Single-shot ultrafast optical imaging needs only one exposure and, thus, is able to record the irreversible transient events. Single-shot ultrafast optical imaging can be classified into 2 categories: the passive detection and active detection, in the light of the sampling methods [25]. Here, the former, called single-shot passive ultrafast optical imaging (SS-PUOI), without the need of an illumination source, is suitable for imaging the targets with self-luminescent and color-selective scenes [26,27]. The latter, called single-shot active ultrafast optical imaging (SS-AUOI), working by imaging the ultrafast events with actively sampling signals, is suitable for imaging low-luminescent or nonluminous targets and scenarios in complex background. Here, we make a review of SS-AUOI on the cutting edge. According to the introduction of Fuller [19], currently, up to 100 million frames per second (Mfps) of frame imaging is already available by commercial electronic imaging, which means that the imaging with a speed of less than 100 Mfps can be directly realized with commercial electronic devices, so we consider ultrafast optical imaging with an imaging speed beyond that of the direct electronic imaging. Accordingly, as Liang and Wang [25] did, this paper also focuses on the ultrafast optical imaging with the imaging speeds within 100 Mfps or frame intervals no larger than 10 ns. The subsequent sections are arranged as followings. In Characteristics of SS-AUOI section, we give characteristic descriptions of the SS-AUOI and then begin our detailed technical reviews in Technical Development of SS-AUOI and SS-AUOI by Computational Imaging sections. We present the prospect of the SS-AUOI in Prospect of SS-AUOI section and, finally, a summary in Conclusions section.

Characteristics of SS-AUOI

The advent of digital cameras [28] has ever made a revolution and pushed a rapid development in high-speed imaging fields. However, there are 2 technological bottlenecks, the data transfer speed and digitalization bandwidth, which limited the further development of the digital camera. To break the bottlenecks, many methods have been developed for SS-AUOI to encode target information so that the sequential images can be recorded with a charge-coupled device (CCD) or complementary metal-oxide semiconductor (CMOS) with no fast response and no high-speed data transfer. SS-AUOI implements its coding using a specially designed pulse [29,30] or

pulse train [31,32] in single-shot acquisition mode so that each of the frame images is sampled by the corresponding subpulse of the special pulse (train). According to the public reports, some of SS-AUOI systems sample the frame images with different sequential subpulses, while others capture the ultrafast imaging through the time–space conversions using the sample pulse to scan the target field of view (FOV).

For the former, the different sequential subpulses see the same FOV, and SS-AUOI cannot resolve the temporal imaging information within a time scale of the subpulse duration. Unlike SS-PUOI regarding frame interval as temporal resolution, SS-AUOI has its temporal resolution to be limited by the sample subpulses. The subpulses also set the maximal effective frame rate at the reciprocal of their time duration [33], instead of the frame interval when the latter is smaller than the former. Accordingly, we would like to assess the frame rate of an SS-AUOI system by its effective frame rate here. At present, the highest effective frame rate has reached 15 trillion frames per second (Tfps) with a 50-fs temporal resolution [33]. For the latter, SS-AUOI works by continuously scanning the sample beam, and its frame number is limited by the exposure time τ_e, which can be characterized by a time function: $G(t)= g(vt) * I(t)$, the convolution between the transition time function $g(vt)$ of the sample skimming over target with a speed of v along the scanning direction, and the sample pulse intensity $I(t)$ in time domain. Accordingly, τ_e shall be no less than the sample pulse duration (τ_p) but tends to τ_p when τ_p is much larger than the transition time Δ/v with a transition distance of Δ. Obviously, here, SS-AUOI still fails to have the exposure time to be less than the sample pulse duration, which means that its effective frame rate still has its upper limit at $1/\tau_p$.

Spatial resolution is traditionally defined by Rayleigh criterion [34,35] and usually checked with a resolving power test target. For SS-AUOI, it shall be calibrated under working state for a single-shot ultrafast imaging system. Consequentially, the spatial resolution shall be checked under dynamic state if some scan is required to transfer the sequential information to spatial domain [36,37], because it will degrade from that under the static state due to motion blur [38]. However, for SS-AUOI, some special coding methods (e.g., spatial–time coding [33] and wavelength–time coding [12,39]) allow it to transfer the temporal information to another domain, e.g., spatial or spectral domain, to avoid the dynamical scan. Resultantly, the spatial resolution under working state becomes equivalent to that in static state, so currently, the available spatial resolution can be less than 833 nm at a frame rate of 0.25 Tfps [39]. In addition, an SS-AUOI system also has its unique dependence among spatial resolution, frame rate, interval time, and FOV depending on the coding method of the sample.

Technical Development of SS-AUOI

SS-AUOI uses laser pulses to probe transient target, which makes it be flexible to encode the sequential information with some physical quantities of the sample pulses. It is worth mentioning that the development of SS-AUOI benefits greatly from the huge progress of laser technology, especially ultrafast laser technology. The excellent coherence and directivity of laser pulse [40] provide great flexibility to encode the probe of SS-AUOI, including space, angle, spatial frequency, and polarization coding. What is more is that ultrafast laser possesses very broad bandwidth [41], which allows converting the time information to spectral domain. In addition, its ultrashort pulse duration and high pulse power bring not only the excellent temporal resolution but also some other novel ways for SS-AUOI, e.g., high-efficient nonlinear frequency conversion [33]. All the advantages above allow SS-AUOI to encode its sample pulses with many methods for ultrafast imaging, which were classified as space division [42,43], angle division [44–46], wavelength division [12,47–49], spatial frequency division [50,51], and polarization division [52]. Among them, the most basic one is space division. Obviously, angle division is essentially of space division. Similarly, spatial frequency, polarization, or wavelength division also works for time–space conversion but is based on spatial Fourier transform, time polarization, or wavelength conversion in advance. Consequently, we review the technological development of SS-AUOI by following categories: space, spatial frequency, wavelength, and polarization divisions. Hereafter, we add an extra section to discuss the SS-AUOI with computational imaging [53,54] due to its special role in the development of SS-AUOI.

Space division

Space division aims at constructing a probe pulse or pulse train so that the different part of the pulse or the different pulse of the train samples targets at different temporal slices but occupies different spatial positions to be recorded. At the early stage of the high-speed photograph, it was usually realized using some spatial scanning designs, e.g., rotating a mirror [55] or electro-optic deflector [56]. However, once the frame interval is required to be down to nanosecond level, spatial scan is hard to work well, so space division begins to be one of the attractive choices.

Space division can be realized either by direct time–space or by time–angle conversion. The former uses the probe pulse (train) to illuminate the ultrafast event and then converts the different sequential images into different spatial positions (direct time–space coding), whereas, in the latter, the pulse (train) illuminates sequentially the ultrafast event by different azimuth angles (time–angle coding). Both of them finally record the images at separated spatial areas.

Direct time–space coding

Among the reported ultrafast imaging setups by direct time–space coding, light-in-flight (LIF) holography and femtosecond time-resolved optical polarography (FTOP) are 2 typical designs. Both of them work for observing light-velocity-moving objects in single-shot mode, where different sequential images record the target at different propagation positions. Some others, e.g., all-optical coaxial framing camera (AOCFC) by parallel coherence shutters [57] and single-shot noncollinear optical parametric amplification (OPA) imaging [33], capture the sequential information at fixed FOV by the frame images.

LIF holography was used to record light in its flight by Abramson [58] in 1978. Unlike the ordinary holography, LIF holography works with light beams with much shorter coherence time, or in LIF scheme, the coherence only occurs when the reference pulse and the object light accurately overlap with each other both temporally and spatially. Its principle is illustrated in Fig. 1A, where an illuminating laser pulse hits a plate that diffuses the light to an optical film [59] or a CCD sensor [60], while a reference pulse is obliquely incident to the recording plane. The reference has its pulse duration at picosecond

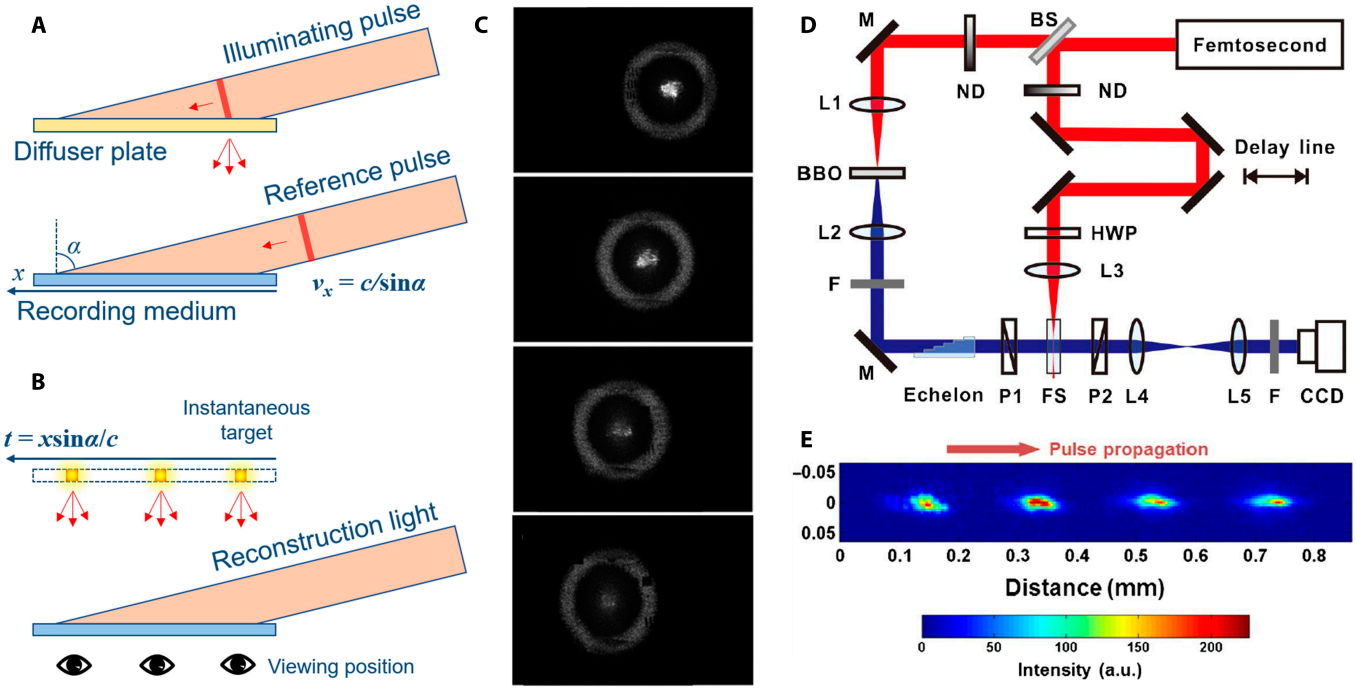

Fig. 1. Schematic of LIF holography for recording (A), reconstructing (B), 4 reconstructed images (C) of light propagation with a frame interval of 192 fs [29], experimental setup of FTOP imaging technique (D) [41], and its 4-frame images of pulse propagation in a fused silica plate (E). a.u., arbitrary units.

or subpicosecond level, and it works equivalently to provide a coherent shutter that moves rapidly and synchronously with the object light. The moving velocity of the reference along the recording medium is $v_x = c / \sin\alpha$ by an incident angle α (c: light velocity in vacuum). This reconstruction can be shown in Fig. 1B. If using a continuous wave coherent light to illuminate the holographic plate at the same angle as the reference pulse, moving the observed position along the medium allows us to see the reconstructed scattering position at a certain moment $t = x \cdot \sin\alpha / c$. Here, the resolved time $\delta t = \delta x \cdot \sin\alpha / c$, which depends on the coherent length (or the spatial width δx of the light pulse along the plate) and the incident angle [29,60]. Figure. 1(C) shows the reconstructed images of a 96-fs 800-nm light pulse propagation. The pulse illuminates a diffuse plate and then overlaps with the reference on the surface of an array detector for $\alpha = 0.5°$. The square image in the center of the brilliant circle is the zeroth-order diffraction image. When moving the observation position from left to right, one can see that the reconstructed light pulse propagates from left to right, which is the same direction as that of the reference light pulse recorded by the camera. The framing images covering 512×512 pixels are recovered from the whole hologram with $4{,}000 \times 2{,}624$ pixels. The framing time is 192 fs with a recording time of 576 fs, and the resolved time is about the reference pulse duration.

LIF holography operates with a scanning-like mode that maps the time onto the length of the recording medium using an oblique incident beam. It is based on coherence gating, so its temporal resolution is relative to the pulse duration. The total imaging time is decided by the length of the whole hologram. The reconstructed time interval can be continuously chosen, which means that large frame number is obtainable. However, the effective frame number is hampered by the reference pulse duration. What is more is that large frame number will result in small frame FOV, which is equal to the total FOV divided by frame number. Apart from visualizing light propagation in air and inside optical media [59–62], LIF holography can also be applied for visualization and image velocimetry of some flows, for instance, the smoke in airflow [63] and wind tunnel [64].

FTOP [22,42,65–67] relies on optical polarography. There, an ultrashort laser pulse acts as the ultrafast flash lighting source, i.e., the probe, and its polarization is modulated by a synchronous pump to a Kerr medium. The FOV is spatially divided into some sub-FOVs, and the corresponding subprobes meet the pump at different moments. Fujimoto et al. [66] realized a single-shot 4-frame FTOP using a quadruple-pulse generator, which combines 4 different probe beams with different optical paths. Later, as shown in Fig. 1D, Yan and colleagues [42,67] used a 4-step echelon to replace the quadruple-pulse generator. Targeted with the pulse propagation in fused silica, Fig. 1E confirmed that FTOP realized 4-frame SS-AUOI with a resolved time of 276 fs and a frame rate up to 1.05 Tfps.

FTOP works on nonlinear optical gating, so its temporal resolution is tied to both the gating pulse duration and the relaxation time of the Kerr effect. As a result, the temporal resolution shall be beyond the gating pulse duration. Here, the echelon plays a very critical role. Its step depth determines the time interval of the subprobes, thereby the frame rate that has an effective maximum equal to the inverse of the pulse duration. The echelon also divides the total FOV to the frame FOV by the step number that directly fixes the frame number. Accordingly, the minimum of the step depth shall be larger than the optical distance within the pulse duration inside the echelon. For a given total FOV, the large frame number corresponds to small frame FOV, thereby the small step width, which may result in strong diffraction of the probe subpulses and cross-talks among the beams from different steps that degrade

the frame images. What is more, for the broadband probe, the use of the transmission echelon with large step number certainly causes strong dispersion unbalance among the subpulses and, thus, limits the temporal resolution.

Compared with LIF holography capturing the diffused light from a scatter, FTOP records the light pulse propagation in a transparent medium, including air [65], liquid [66,67], or solid [42], which can be induced by some nonlinear birefringence. However, FTOP needs strong enough third-order nonlinear effect, so its pump intensity is required to be higher than that of LIF holography.

AOCFC [57] realized its time–space coding with some beam splitters. It records ultrafast events with cameras by parallel coherence shutters operating at different moments, as shown in Fig. 2B. Figure 2A presents the scheme of AOCFC, where the pulse laser with 10-ps duration and 527-nm wavelength is divided into a sample light and a reference light. The sample becomes a pulse train possessing 4 subpulses with an interval time of 34 ps using a pulse train generator including mainly 3 splitters. The sample passes through the ultrafast target and then is divided into 4 replicas. Meanwhile, the reference is also divided into 4 subpulses with designed time delays and then combined with 4 corresponding probe replicas, respectively. The 4 groups of the combined beams form spatially separated holograms and are imaged on the different areas of a CCD camera. Figure 2C displays 4 recorded frames at the relative instants: −120, −86, −52, and −18 ps, targeted with the discharge formation from an aluminum foil driven by laser pulse. The corresponding areal electron densities are retrieved as shown in Fig. 2D.

There are several differences between AOCFC and FTOP. First, AOCFC has not divided the FOV, and every frame is coaxial and shares full FOV. Second, AOCFC records the ultrafast evolution rather than the light–velocity motivation just like FTOP. Third, the linear coherence shutter mechanism, thus, has a much lower light intensity requirement compared to the nonlinear shutter. Moreover, hologram imaging makes us accurately obtain the phase distribution. Although increasing frame number does

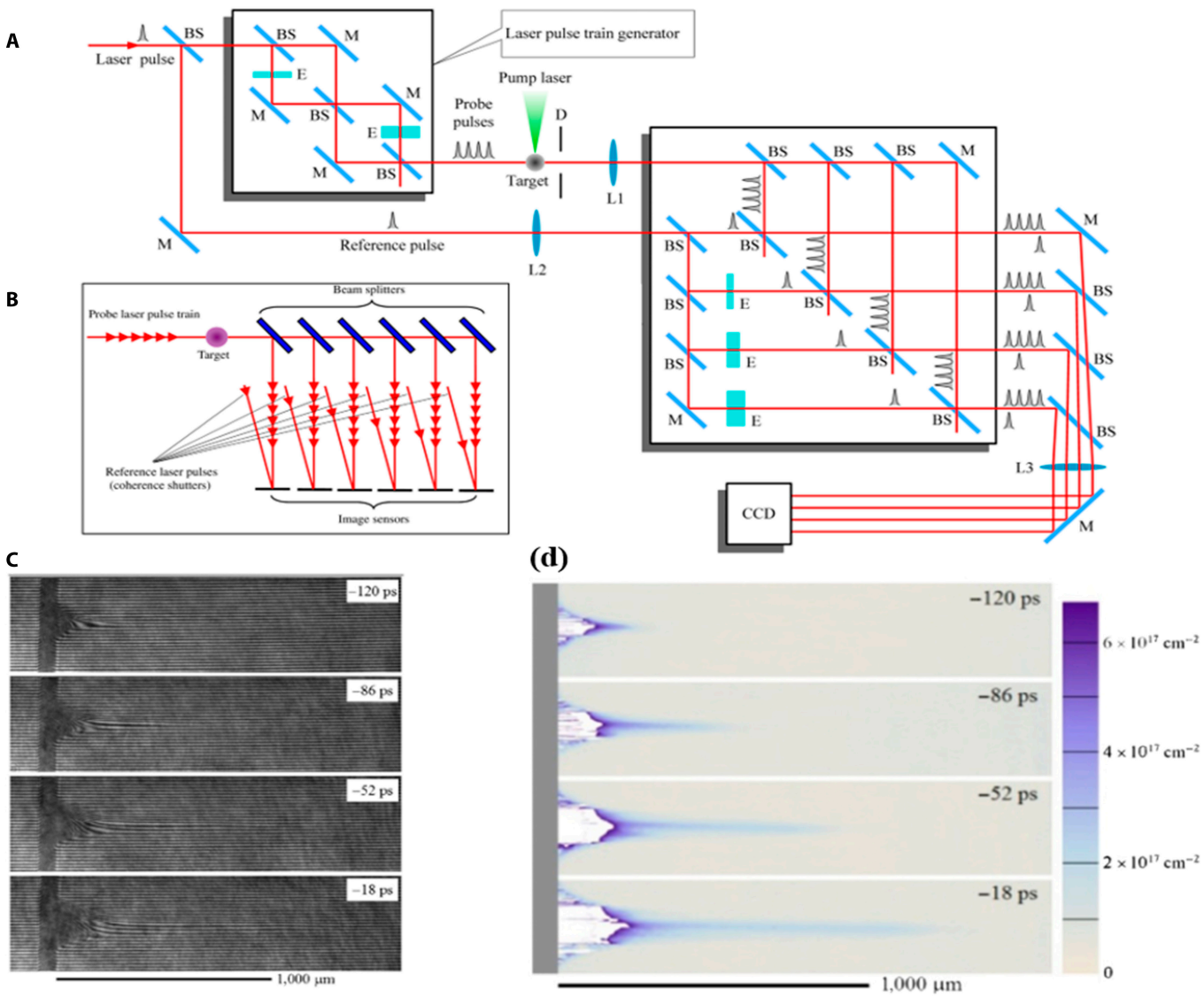

Fig. 2. Schematic diagram of AOCFC (A), optical diagram of the parallel coherence shutters (B), 4 holograms at −120, −86, −52, and −18 ps (C), and the retrieved electron areal density (D) [57].

not narrow the FOV of AOCFC, it can degrade the modulation of the holograms and increase the system complexity.

Noncollinear optical frequency conversion can also be used to realize time–space coding for ultrafast imaging. The phase-matching requirement for frequency conversion allows us to map one light beam information to another. The noncollinear design can work to convert a sequential signal into a series of separate spatially information. Its principle is illustrated in Fig. 3A, where a sampling pulse carrying sequential information passes through some cascade optical imaging converters. A serial of ultrashort triggers with tunable relatively time delays to trig their imaging converters and, thus, to switch transiently the sequential signal to a noncollinear spatial information. Our group reported framing imaging based on noncollinear OPA (FINCOPA) [33] in 2020, where some noncollinear optical-parametric amplifiers serve as the optical imaging converters for time–space coding by noncollinear OPA. In the proof-of-concept experiment, the triggers are some ~40-fs, 400-nm pulses with tunable time intervals, while the sample is an 800-nm pulse whose time duration is chirped to 50 ps for covering totally the target event. The target is an air plasma grating formed by focusing a pair of 40-fs, 800-nm pulses by an adjustable crossing angle so the grating can be tuned with its spatial period down to 10 μm and a lifetime of picoseconds. Figure 3B is the recorded sequential images in the single-shot mode at 4 moments from 0 to 30 ps, where clearly presents the dynamical evolution of the plasma grating with a spatial modulation period of 12 μm (which was enhanced to ~2 μm with a 20× objective lens) and an effective frame rate up to 15 Tfps.

FINCOPA has high OPA gain, so it is qualified for the imaging under weak signal. Its frame number, temporal resolution, and frame rate are only determined by the stage number of the parametric amplifiers, the trigging pulse duration, and the relative delay between the triggers and the sample pulse. Its spatial resolution is mainly relative to the OPA spatial bandwidth, and effective optical aperture of the imaging system, respectively. Interestingly, its frame number, frame rate, temporal resolution, and spatial resolution are independent with each other, which bring great flexibility for the system design and large promotion space in the time/spatial resolutions and frame rate. Moreover, all the frame images of FINCOPA are coaxial and without view parallax. FINCOPA is based on nonlinear frequency conversion, so it has an inherent advantage applicable in some spectral zones beyond the visible and near infrared (NIR), e.g., the mid-infrared (MIR) [68,69]. However,

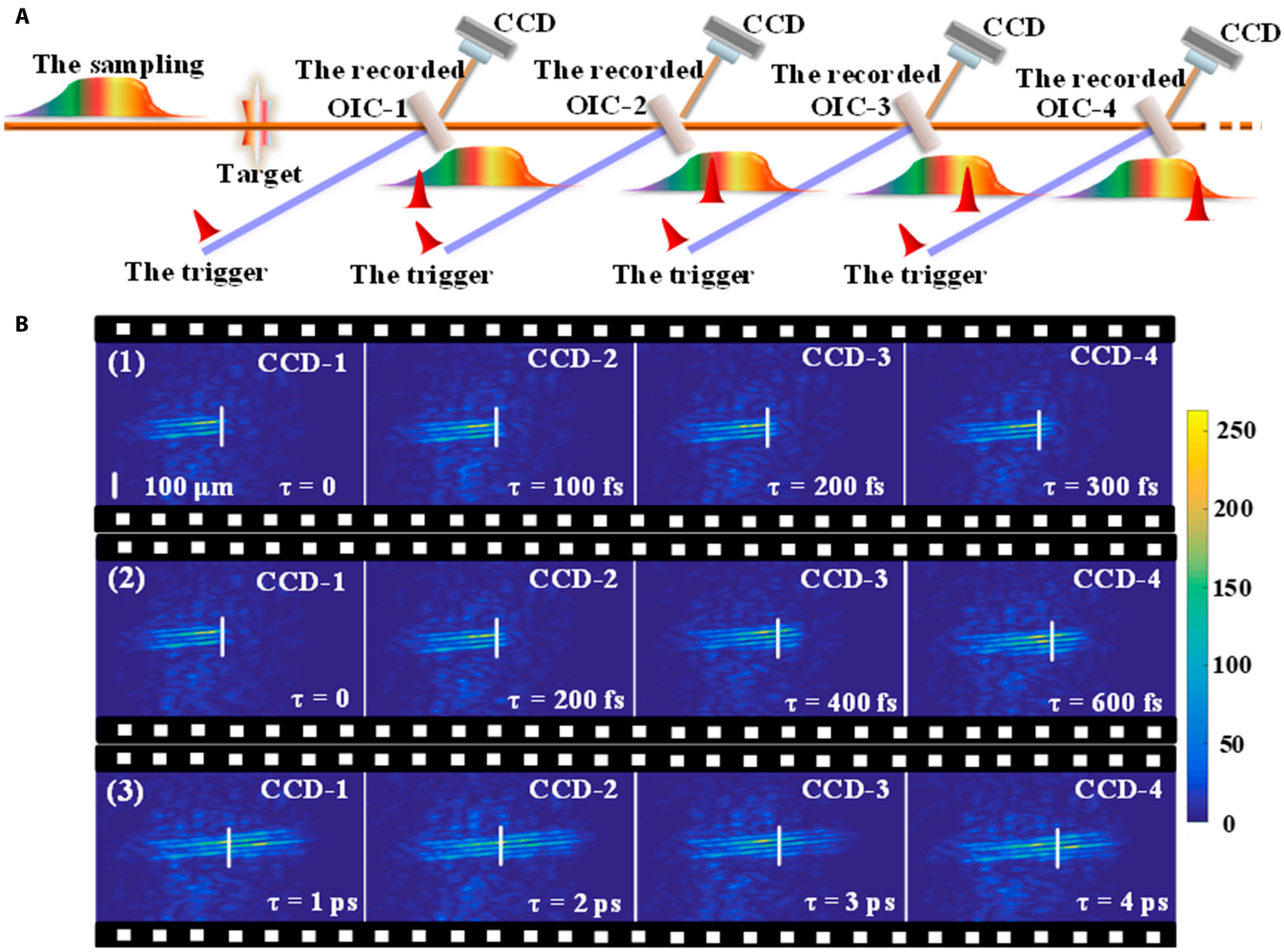

Fig. 3. The FINCOPA system based on time–space coding [33]: (A) principle of FINCOPA, optical imaging converters (OIC-1 to OIC-4), and (B) 4 images recorded in the single-shot mode at 4 moments.

in current design, increasing the frame number means more stages of the parametric amplifiers required, which makes FINCOPA be more complex and difficult to operate, and higher pump energy needed. However, because of its femtoseconds of temporal resolution, micrometer-level spatial resolution, and more than 10 Tfps frame rate, FINCOPA is qualified for the ultrafast evolutions from femtoseconds to picoseconds and the spatial features as fine as micrometers in the areas, such as ultrafast laser plasma physics [70] and precise laser machining and fabrication [71].

Time–angle coding

Space division can also be realized by time–angle coding, where multiple pulses with different time delays are used to illuminate the ultrafast process by different azimuth angles [72,73], so the sequential images can be separated spatially on the image plane. Wang et al. [73] realized a pulsed digital microholography by time–angle coding and successfully recorded an ultrafast process with a visible spatial structure of about 10 μm. The temporal resolution was 50 fs, and a frame interval was 300 fs. The frame number was set at 3, which is difficult to be increased for this design because the frame number increases sharply with the complexity of the system. Later, by use of 2 sets of 2 × 2 mirror arrays for time–angle coding, Yeola et al. [74] realized a 4-frame SS-AUOI with a temporal resolution of 30 fs and a frame rate beyond 30 Tfps. This design is more compact than that by Wang et al. [73], but it is still difficult to have a larger frame number.

Recently, a minireflector delay-line array [75] was integrated with an array of minireflector and an array of micrometer lead with the mini cardan joint to generate multiple back-reflected subpulses with some adjustable propagation angles and delay intervals. By using minireflector delay-line array, a single-shot ultrafast hologram on time–angle coding [75] was developed as shown in Fig. 4, which increased the frame number up to 9, meanwhile having a frame rate of 7.5 Tfps. This scheme can accomplish SS-AUOI by both amplitude and phase information. Its temporal resolution depends mainly on the original laser pulse, while the signal-to-noise ratio and accuracy of its images are affected by the in-line hologram with an iteration algorithm.

Echelons were used as compact time delayers [31,76] for single-shot time–angle coding of ultrafast imaging together with some focusing optics. Frequency domain integration sequential imaging (FISI) [77] is a typical example as shown in Fig. 5A. In its probe path, an echelon combined with a lens array is used to split the probe into multiple daughter pulses that are guided by a lens to illuminate the ultrafast event at different angles. Because the daughter pulses experience different optical distances inside the echelon, they sample the event at different moments and then are imaged by another lens and another lens array to recording surface. The recorded shadow images of an air plasma channel are shown in Fig. 5B with 79-fs frame interval and 65.9-fs exposure time. Figure 5C presents another similar design to FISI, called "single-shot nonsynchronous array photography" (SNAP) [76]. There, the probe pulse is split by a diffractive optical element (DOE) into an array of angled daughter pulses whose pulse fronts are orthogonal to the optical axis. The daughter pulses are then imparted with different time delays by an echelon to probe the ultrafast event in rapid succession and finally imaged onto different regions of a camera by a microlens array. In SNAP, the illumination fronts keep flat,

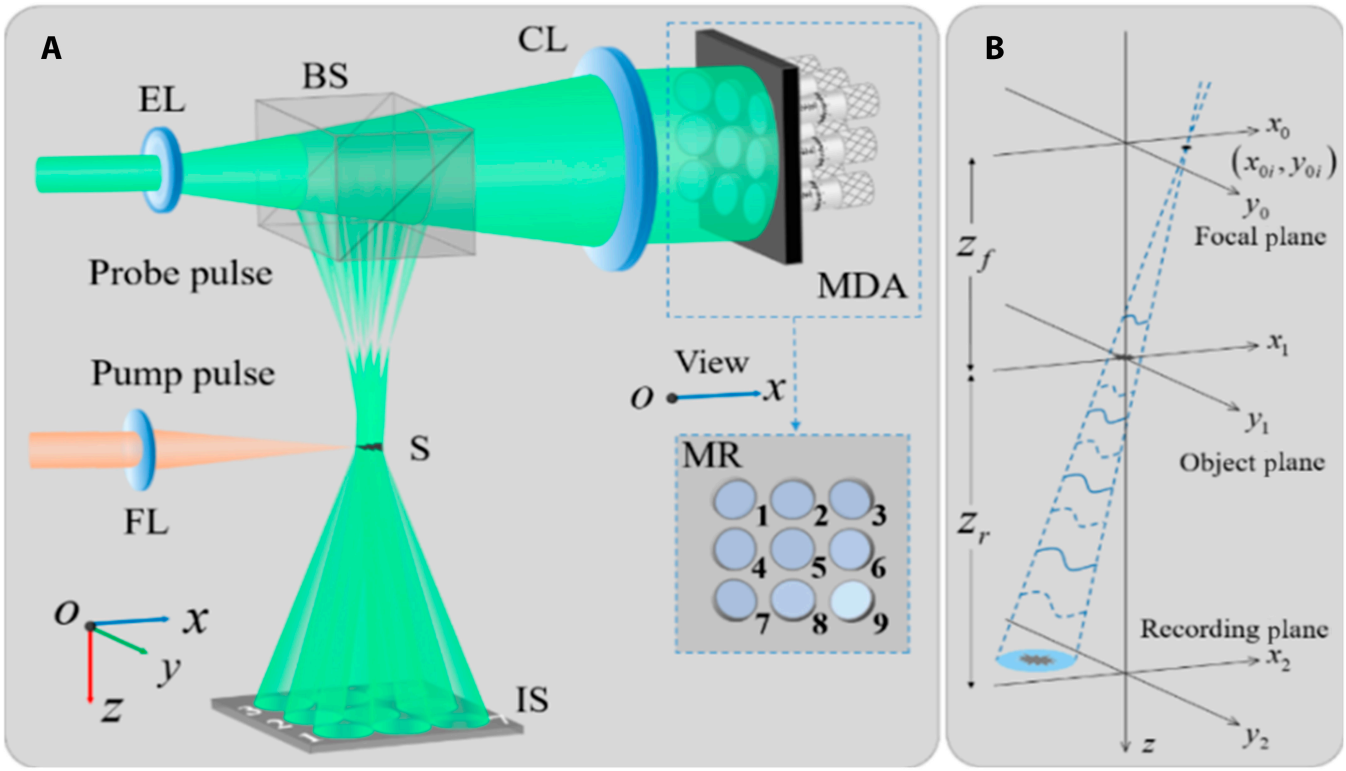

Fig. 4. Layout of single-shot ultrafast hologram on time–angle coding (A) and the coordinate systems of the in-line holography (B) [75]. MDA, minireflector delay-line array; BS, beam splitter.

independently of beamlet angle, or SNAP can realize "global shutter". Figure 5D confirmed that SNAP can record more than 20 frame images of a laser-induced plasma filament at an average rate of 4.2 Tfps and a peak rate of 5.7 Tfps.

Time–angle coding allows different probe beams to pass through the event at different angles, so the frame images have parallaxes compared with the coaxial sampling [33]. Meanwhile, the noncollinear design also suffers from the synchronization difficulty and the experimental calibration of the frame intervals despite that the echelon has a designed step size. As the frame number increases, the dispersion imbalance among the probes of the frames will become serious and, thus, degrade the temporal resolution due to the use of the transmission echelon. The imaging in time–angle coding technique is based on shadow imaging, which makes it be suitable for the snapshot of the processes with rapid variations of refractive index or absorption coefficients, e.g., optical Kerr effect, Coulomb explosion, laser-induced plasma, and thermoelastic wave [78].

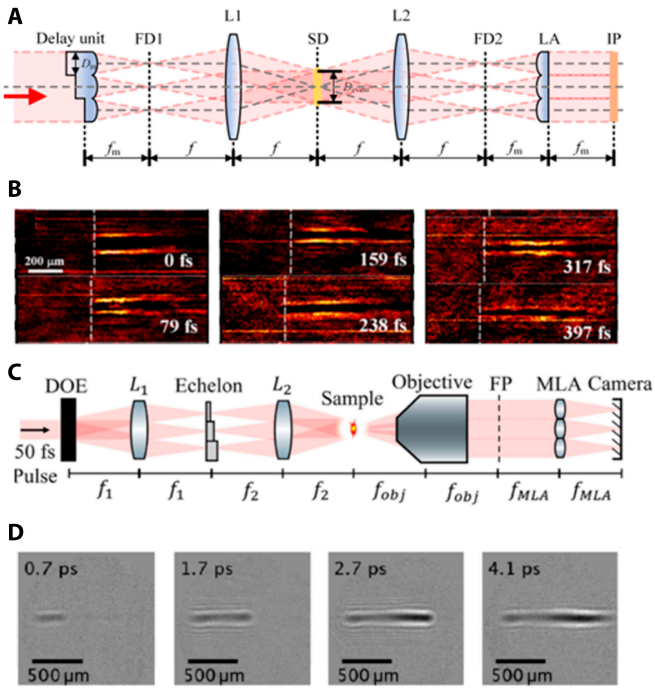

Fig. 5. Layout of FISI system (A) and its shadow imaging of an air plasma channel with a frame interval of 79 fs (B) [77] and the layout of SNAP system (C) and its evolution images of a laser-induced filament (D) [76].

Spatial frequency division

Different from space division, where the sequential frames correspond to the images at separated areas, spatial frequency division relates a unique carrier spatial frequency to individual time slice [51,79,80]. Here, the probe beams may be spatially overlapped at the surface of the camera, but in the succeeding image restoration, images at different times are loaded on different spatial carrier frequencies, so the sequential images can be recovered by extracting corresponding information in spatial frequency domain. Liu et al. [81] reported the holographic recording of an air-discharge event by spatial frequency division in 2002 with 3 frame images with 5.9-ns temporal resolution and 12-ns frame interval. Moon et al. [79] presented an interesting structure of single-shot sequential holographic imaging (SSSHI) in 2019. Figure 6A shows the optical system seeded by a 30-fs, 800-nm laser system. The pulse is split into 5 sequential subpulses by 10 beam splitters (S1 to S10) and 5 pulse delayers (PD1 to PD5). By using 5 diffraction gratings (G1 to G5), these subpulses evolve into 2 pulse trains: a coaxially propagating pulse train composed of 5 zeroth-order pulses from the gratings and an off-axis propagating pulse train, corresponding to the high-order pulses diffracted from the same gratings. The former works as reference pulses, while the latter does as the object lights for the holography. The probes sequentially sample the tested object and then are imaged by an objective lens and a tube lens onto the plane of an image sensor. Meanwhile, the references pass through a 4-*f* imaging system consisting of 2 lenses (L1 and L2) and finally congregate and overlap with the probe beams on the Iris (IS) plane. Consequently, an off-axis hologram can be recorded by spatial frequency division containing 5 groups of interference fringes with the same fringe period and different fringe orientations. Figure 6B confirmed experimentally that 5 frame images are recovered from the recorded spatial spectrum of the holographic images by traditional spatial filtering algorithms [82], which carry both amplitude and phase target information at different time slices. Figure 6C displays the ultrafast holographic sequential imaging with a frame rate of 5 Tfps to visualize the dynamics of laser-induced air plasmas.

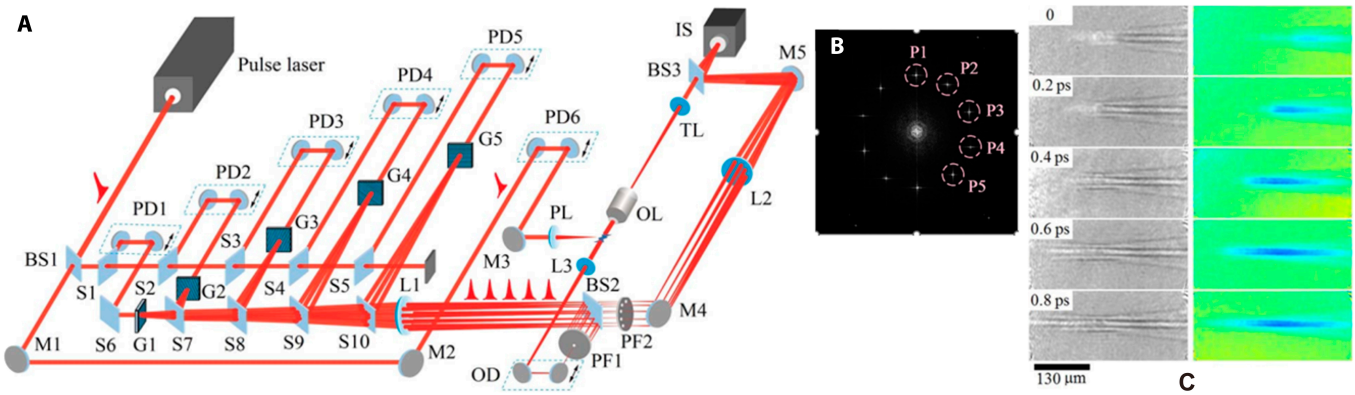

Fig. 6. Optical layout of the SSSHI system (A), the spatial Fourier spectrum of the hologram (B), and ultrafast sequential holographic imaging of a femtosecond laser-induced air plasma (C) [79].

Compared with other SSSHI methods [32,63], the setup can overcome the walk-off effect occurring usually in off-axis holography and, thus, effectively avoids the influence from the short coherence of ultrashort pulses on FOV (or spatial resolution). Meanwhile, it has a relatively simple and easy synchronization alignment. In this setup, the recording plane and all the positions of the gratings satisfy image-forming condition, so the interference fringes from each spectral component can match the whole pulse spectrum, which allows the holograms to get optimal contrast.

Frequency recognition algorithm for multiple exposures [51], called FRAME, is another similar approach to realizing spatial frequency division by modulating a train of sample pulses with different orientations of stripe intensity patterns as structured illuminations to the target scene. Figure 7A is the experimental setup, which aims to record light propagation inside a Kerr medium (CS_2). The illuminating pulse is firstly divided into 4 subpulses, which are temporally controlled via separate optical delay lines. Then, the 4 subpulses are superposed with a structural code to encrypt a single event, which is decoded later. As a result, the different subpulses carrying with different sequential information will locate in different spatial frequency domains, which means that the spatial Fourier spectra of the sequential images can be recorded with separated spatial regions. After spatial filtering, it is easy to reconstruct the frame images. Figure 7B shows the recorded images captured at 1, 2.5, and 5 Tfps, separately, with a resolved time as short as 200 fs. Here, the coding strategy enables laser probing with arbitrary wavelengths and bandwidths to gather signals with indiscriminate spectral information in order for ultrafast videography with full spectroscopic capability. Accordingly, both the temporal resolution and the minimal frame interval are only decided by the laser pulse duration.

TSFM, an ultrafast imaging microscopy working by time and spatial frequency multiplexing [80], is a single-shot ultrafast microscopy that can record more than 12 frames at a time with a frame rate of 5 Tfps. As shown in Fig. 8A, in TSFM, a spatial light modulator (SLM) written with a 2-dimensional (2D) diffraction grating pattern was used to split the laser pulse into multiple subpulses propagating with different angles, while a custom-made echelon was added to a designed temporal delay to each subpulse. We can see that TSFM records the interference between these reference pulses and a sample pulse by time and spatial frequency coding and realizes its single-shot imaging by retrieving the stroboscopic images from the interference. Figure 8B shows the sequential images of a 100-fs light pulse passing through milk, a turbid medium, with a frame rate of 5 Tfps and a spatial resolution of 8.0 μm. The frame number is 14 with an optimal temporal resolution that can be estimated by the pump pulse duration. However, here, increasing the frame number will degrade both the signal-to-noise ratio and the spatial resolution of the recorded images.

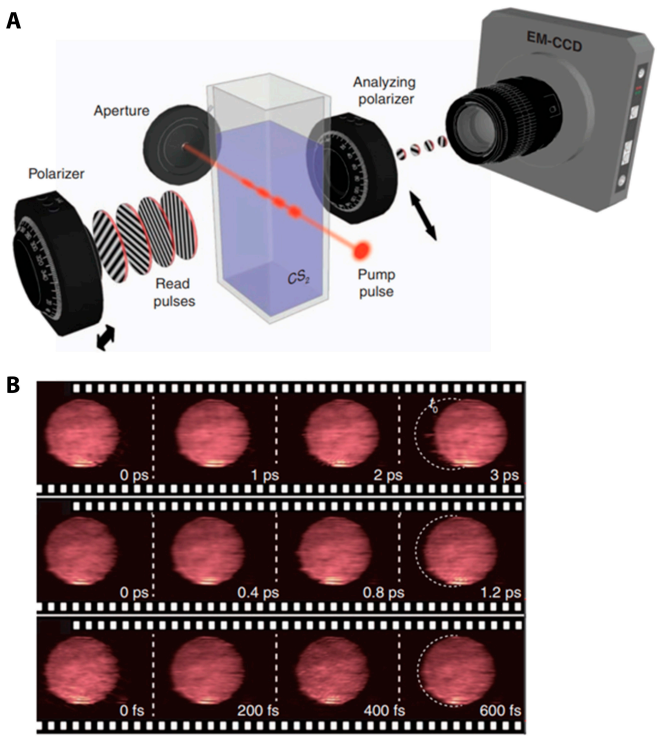

Fig. 7. Setup of FRAME system (A) and the recorded and reconstructed images of a laser pulse propagating in a Kerr medium by the frame rates of 1, 2.5, and 5 Tfps (B) [51]. EM-CCD, electron multiplier CCD.

Wavelength division

Wavelength division is one of the mainstream technologies of SS-AUOI for the transient targets with a time scale from femtoseconds to nanoseconds. It is well known, for an ultrashort laser pulse, that one of its inherent properties is its broad spectral bandwidth, which allows SS-AUOI to implement time–wavelength coding by some dispersion managements [83]. First, SS-AUOI uses an ultrashort laser pulse as the probe to sample transient scene so that the spatial imaging information at a specific time point is carried by corresponding spectral components. Then, the probe is spectrally separated into some subpulses using some dispersive optical elements or spectral filters, so the different sequential images are carried by the spatially separated subpulses and recorded by commercial CCD cameras. That is, wavelength division allows SS-AUOI to transfer the sequential information to spectral domain and finally to spatial domain to avoid the limitation from the time response of the recording media. Here, the measurable time window depends on the probe pulse duration, which can be easily stretched to picoseconds [84,85], even nanoseconds [86].

In 2014, K. Nakagawa et al. [87] proposed an SS-AUOI system based on time–wavelength coding, called "sequentially time all-optical mapping photography (STAMP)" [88]. As shown in Fig. 9A, STAMP has a temporal imaging module consisting of a pulse stretcher and a pulse shaper. The former widens the probe pulse up to picoseconds even to nanoseconds by managing spectral chirps. Then, the pulse shaper modulates further the probe into some wavelength-coded sequential pulse train to probe the ultrafast target. After the target, a spatial imaging module is used to separate spatially the wavelength-coded pulse train into different subpulses. Therefore, the ultrafast target information at different times becomes separated in space to be directly recorded at different areas on a surface of the used CCD camera. Figure 9B presents the recorded 6-frame sequential images of the STAMP system with a frame rate of 4.4 Tfps. The temporal resolution and spatial pixel resolution are 733 fs and 450 × 450 pixels, respectively.

However, the use of a periscope array greatly complicates the STAMP system and, thus, limits the imaging only to

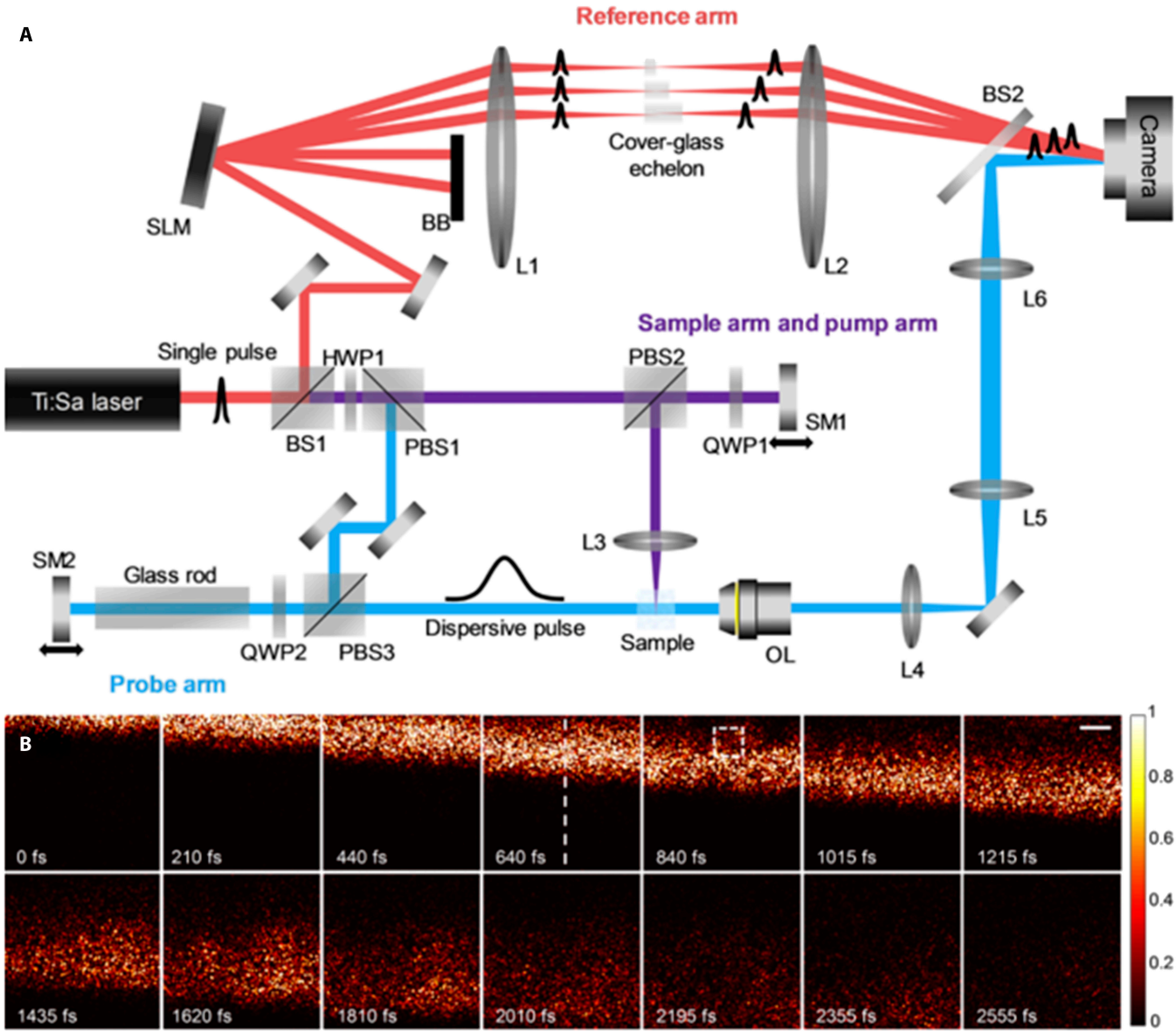

Fig. 8. Experimental setup of TSFM (A) and the sequential images of a light beam traveling through milk, a turbid medium (B) [79].

6 frames. Some efforts have been made to promote the frame number. With a specially designed DOE and a band-pass filter [12], the spectral filtering STAMP (SF-STAMP) has pushed the frame number to 25 frames. Lens array STAMP with a microlens array instead of the DOE for hyperspectral imaging has gotten 24-frame images acquisition with 1-μm spatial resolution [89]. However, in all the STAMP systems above, the time–wavelength coding images were spatially separated at different areas of a detector by a 4-*f* system as the spatial mapper, resulting in a confliction between the frame number and the frame pixel number. To further increase the frame number without sacrificing pixel resolution, a branched 4-*f* system was specially designed to branch the probe into 2 paths using a slicing mirror as shown in Fig. 10A [90] with multiple facets tilted by different angles. Figure 10B shows that the branched path allows us to capture dynamic events by 2 CCD cameras. Figure 10C presents the 18-frame sequential images of femtosecond laser-induced filament with 2 detectors, each of which captures 9 frames, so the STAMP with a branched 4-*f* system doubles the frame number without sacrificing the pixel resolution. However, the slicing mirror locates at the Fourier plane along the long edge but at the image plane along the short edge, which leads to a degradation of the spatial resolution. To overcome this limitation, a hybrid-plane spectral slicing for STAMP [91] was developed, which introduces a spatial mapping module with an asymmetric optical design to set the slicing mirror in the hybrid plane of the system as shown in Fig. 11A. Figure 11B exhibits the captured 12-frame images of the laser interacting with air and water by a frame rate of 1.18 Tfps, confirming the balanced but good imaging quality along 2D spatial directions.

However, most of the STAMPs need some complex and bulky optical devices, such as a pulse stretcher and a pulse shaper, are not so user-friendly, and exhibit low flexibility regarding the control of frame rate and exposure time. To address the issues, an improved SF-STAMP [92] was reported, which, named acousto-optic programmable dispersive filter-based SF-STAMP.

It integrates SF-STAMP scheme with the acousto-optic programmable dispersive filter plus digital in-line holography to enable independent control of frame rate, imaging intensity, and exposure time with a simple system design. This technique can be easily switched between different time scales from picosecond to nanosecond regime. The use of digital in-line holography without any reference leads to a very high technical simplicity.

Despite the great performances of the STAMP-based systems in frame rate, frame number, and spatial resolution, all of them work by wavelength division, which means that different frame images occupy different spectral bands, so increasing frame number will hurt temporal resolution, thereby limiting the effective frame rate. For example, the temporal resolution is 733 fs for STAMP [87] or 465 fs for SF-STAMP [12], so the effective frame rate shall be 1.37 or 2.15 Tfps, rather than 4.4 or 7.5Tfps for STAMP or SF-STAMP, respectively.

Also aiming to extend the time window of SS-AUOI to nanoseconds, another STAMP system was developed by Nemoto et al. [93], with an interesting design: a free-space angular-chirp-enhanced delay (FACED) [94,95]. FACED consisted of a grating, a pair of tilted mirrors, and a 4-*f* system. As shown in Fig. 12A, it can offer a linear frequency-to-time mapping in any wavelength with a time scale up to nanosecond level. By integrating it with SF-STAMP, an SS-AUOI based on time–wavelength coding has been developed, as presented in Fig. 12B. By using this setup, a 6-frame imaging has been implemented with a time window of 1,516 ps, and the corresponding average frame interval is 303.2 ps, as shown in Fig. 12C. Despite this, for SS-AUOI with a required time scale up to nanosecond level and a temporal resolution of hundreds of picoseconds, it is unnecessary to use a broadband probe and the grating 4-*f* optical system-based setup for

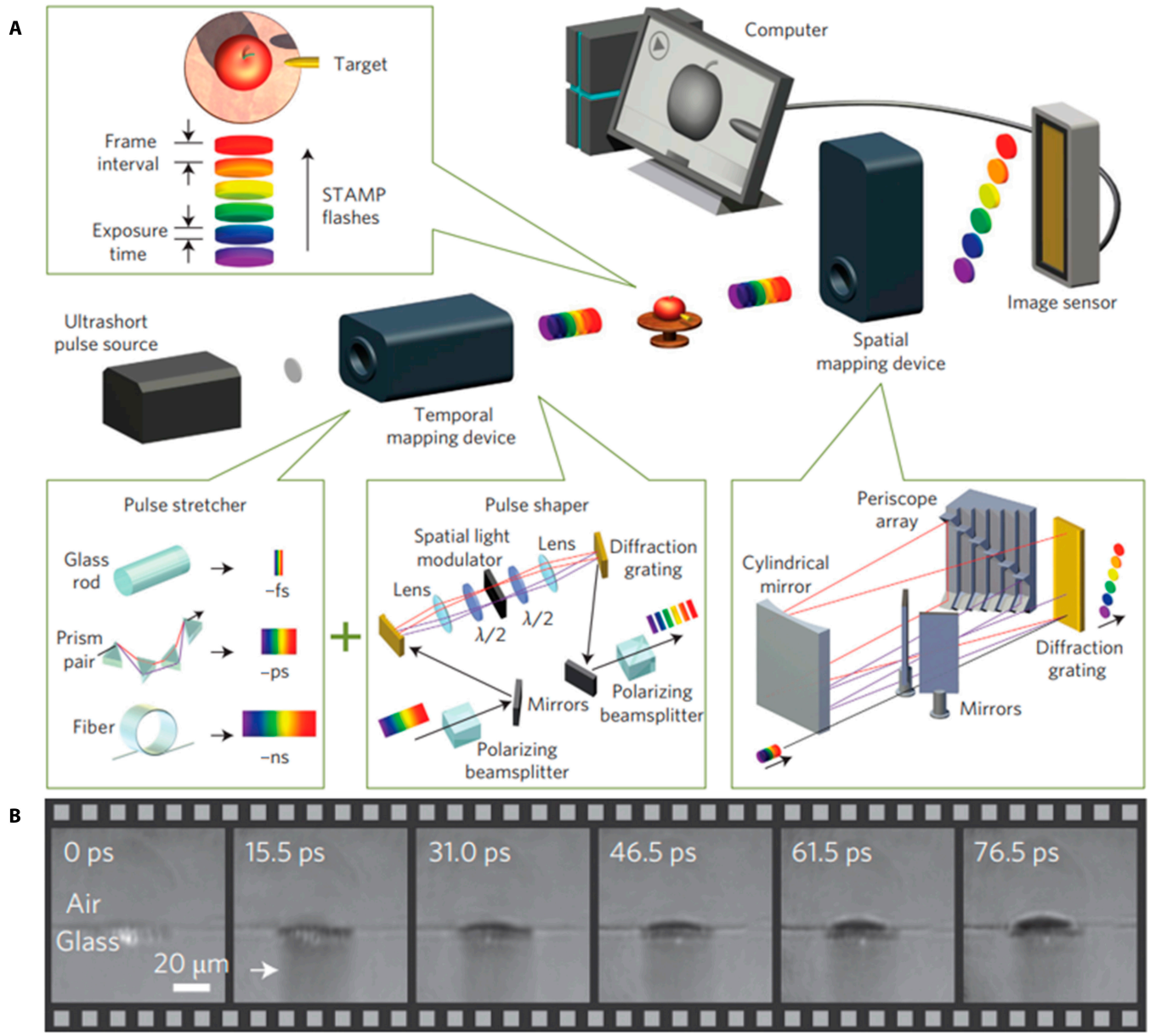

Fig. 9. Setup of STAMP (A) and 6 sequential images of an ultrafast laser-induced filament (B) [87].

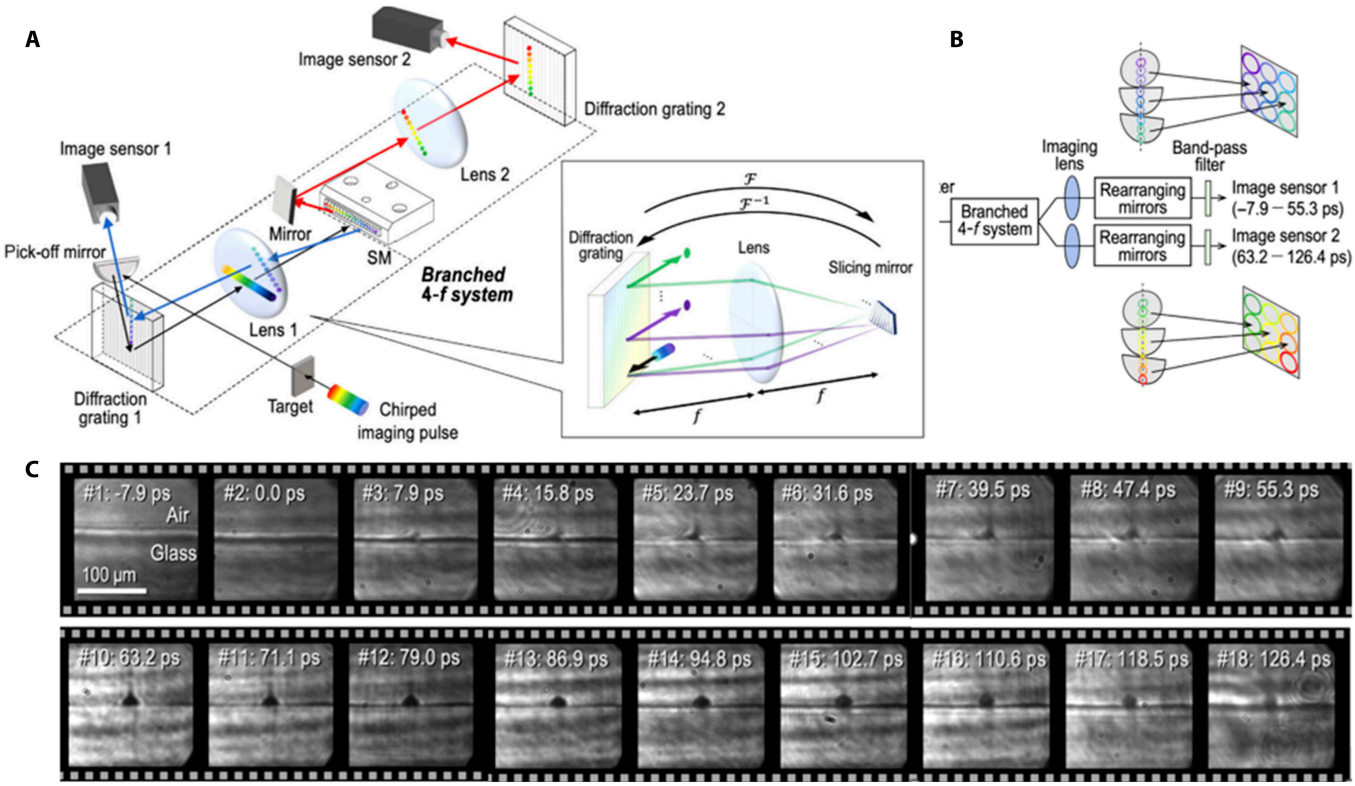

Fig. 10. Experimental setup of STAMP (A), the branched optical arrangement to capture dynamic events (B), and the sequential images of ultrafast laser-induced filament (C) [90].

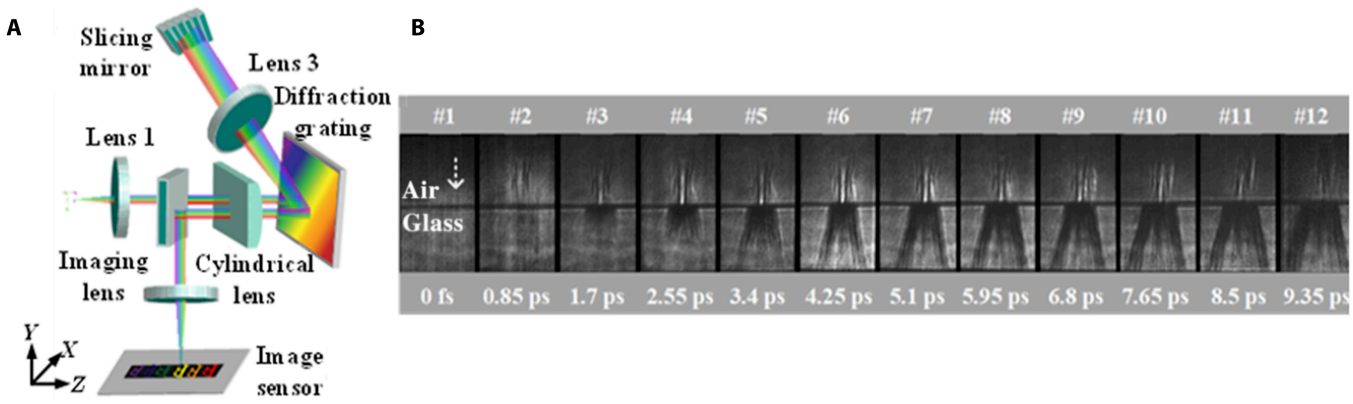

Fig. 11. Spatial mapping module of hybrid-plane spectral slicing for STAMP (A) and the sequential images of femtosecond laser-induced filament (B) [91].

time–wavelength coding. On the other hand, if the temporal resolution is required to be at femtosecond or several picosecond level, the frame number shall be very large, e.g., some hundreds of order, to ensure small enough frame interval, which will be difficult for FACED.

All-optical photography with a raster principle (OPR) [96] was reported in 2021, which combined raster imaging with time–wavelength coding method to push a frame rate to 2 Tfps. Figure 13A shows that OPR system consists of 2 parts: data acquisition and reconstruction. Figure 13B exhibits the detail process of the data acquisition by time–wavelength coding. A temporally stretched pulse samples the target and then is incident into the first imaging system that includes an objective lens and a microlens array to segment the beam and form some raster images. The raster images are situated at the front focal plane but are recorded by a CCD sensor at the rear focal plane of the 4-*f* imaging system. By setting a diffraction grating at the Fourier plane of the 4-*f* system, the raster images are spectrally dispersed at the surface of the CCD. After the data acquisition, the sequential information is extracted from data of the raster images sorted by different spectral components and constructed into multiple images by a Fourier transform algorithm. By using the plasma dynamics in air and silica glass as targets, OPR system has gotten 12-frame images with a spatial resolution of 90 line pairs (lp)/mm or 1,236 × 1,626 pixels. The frame rate and the temporal resolution are 2 Tfps and 460 fs, respectively.

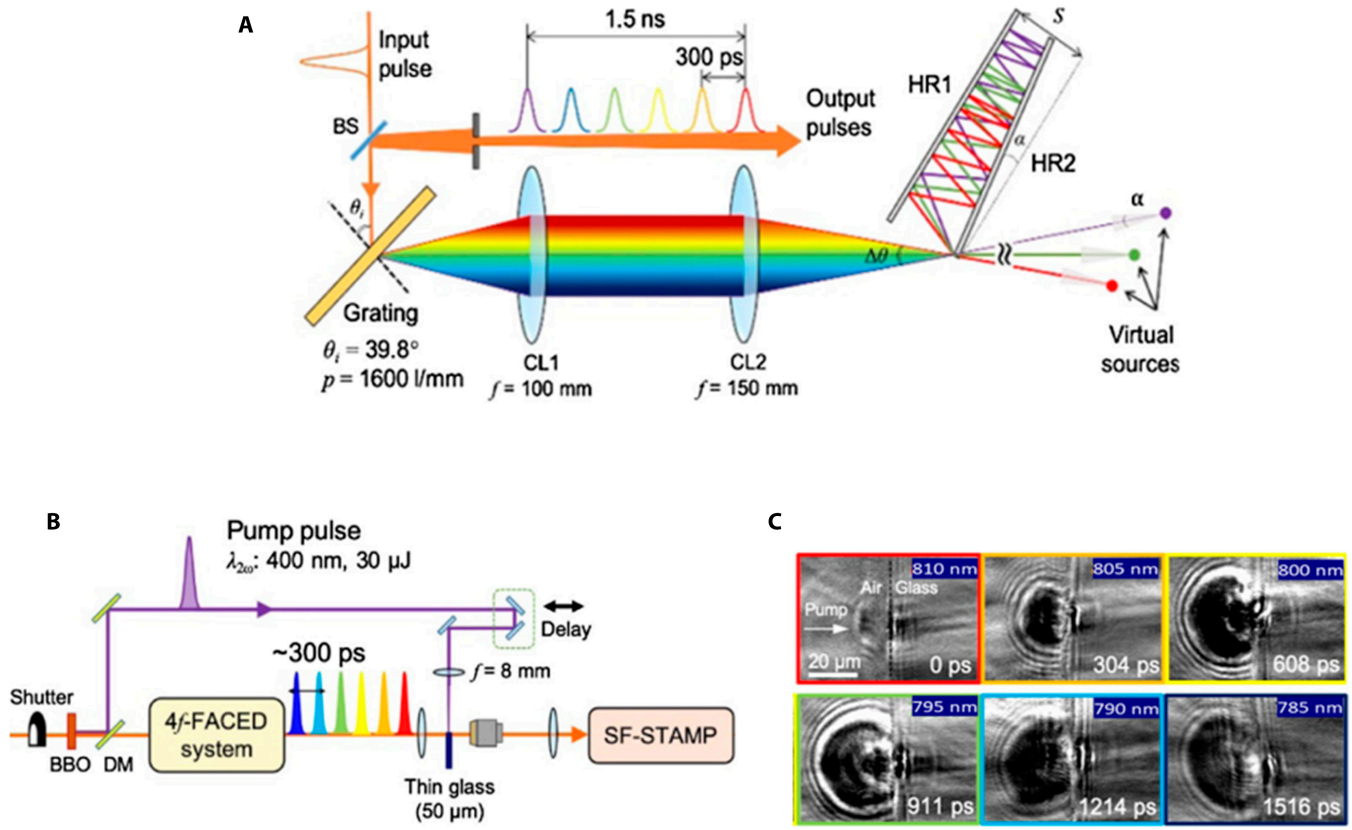

Fig. 12. The setup of spectrally sweeping pulse generation 4-*f* FACED system (A), experimental setup of single-shot 6-frame imaging system (B), and the captured images of femtosecond laser ablation process on glass surface (C) [93].

OPR system is simple and compact. Its pixel resolution depends on the number of the raster images. However, OPR, the same as other methods based on time–wavelength coding, is restricted by the uncertainty relationship between time and wavelength. What is more is that, in OPR, there exist some colors smearing on the image plane, which may degrade the spatial resolution.

Single-shot frequency domain tomography (FDT) [97] presents a unique design to realize time–wavelength coding for the evolving light-velocity objects. In FDT, some long pulses are used to sample the whole process of the ultrafast event, simultaneously, to measure the projected views of the target in different directions. By applying Radon transformation in spatiotemporal domain, FDT allows to reconstruct the sequential images by some well-established methods, e.g., x-ray computed tomography (CT). Essentially, FDT integrates noncollinear frequency domain hologram (i.e., frequency-domain streak cameras [77]) and CT to extend the (x, t) imaging to (x, z_l, t) imaging, where $z_l = z - vt$ is the local longitudinal axis with the propagation velocity v. The imaging frames at (x, z_l) plane are retrieved using Radon transform. FDT records the pictures at different angles for tomography to retrieve the distribution of the image at z axis, but its time dimension is encoded to wavelength on the basis of frequency domain hologram [43], which is different from the time–angle coding methods, where the time dimension is directly encoded to the angle to realize spatial separation of the frame images.

Figure 14A is the experimental setup of FDT. The aim is to capture the evolution of the nonlinear refractive index envelope from Kerr effect excited by a 100-fs, 800-nm laser pulse. Two 800-nm pulses with a small crossing angle hit onto an HZF4/BBO/HZF4 sandwich to generate 15 probe pulses at 400 nm by nonlinear frequency conversions, e.g., frequency doubling, 4-wave mixing, and so on. Five of the 15 probes are selected to sample the ultrafast target by different incident angles collimated by a lens and then imaged by another lens into an imaging spectrometer. The probe pulses interfere with a reference pulse in the spectrometer to form a 2D interferogram with the fringes in spectral and 1D spatial domains as shown in Fig. 14B. By 2D Fourier transforms and filtering, phase streaks at different angles can be obtained. The selected snapshots at (x, z) of the nonlinear index profile with a time interval of 2.4 ps are retrieved from the phase streaks using tomographic algorithms, as shown in Fig. 14C.

In the time dimension, FDT is a continual recording technique, so the choice of the frame time points is more flexible compared with FTOP or FISI. In FDT, the project beams extracted by different spatial frequencies. Large enough beam number is required for high transverse spatial resolution. Moreover, the sparse angular sampling may result in distortion of the retrieved images.

Compressed ultrafast photography (CUP), reported by Gao and colleagues [26] in 2014, has drawn great attention in optical imaging fields [98–102]. It originally works with passive detection mode and has gotten great successes in large frame number [26] and high frame rate [100] with a simple configuration [103]. Fortunately, CUP can also work with active detection mode. "Compressed ultrafast spectral–temporal

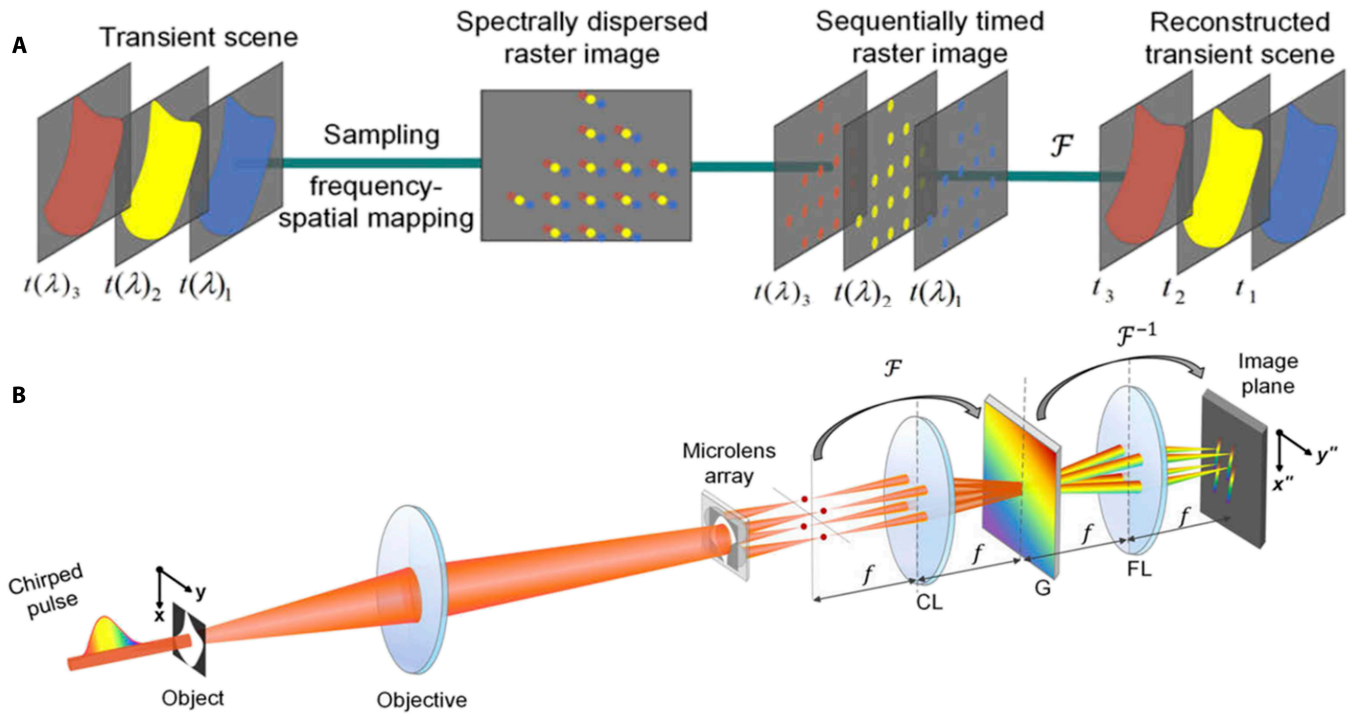

Fig. 13. The principle (A) and the setup of the raster framing camera (B) [96].

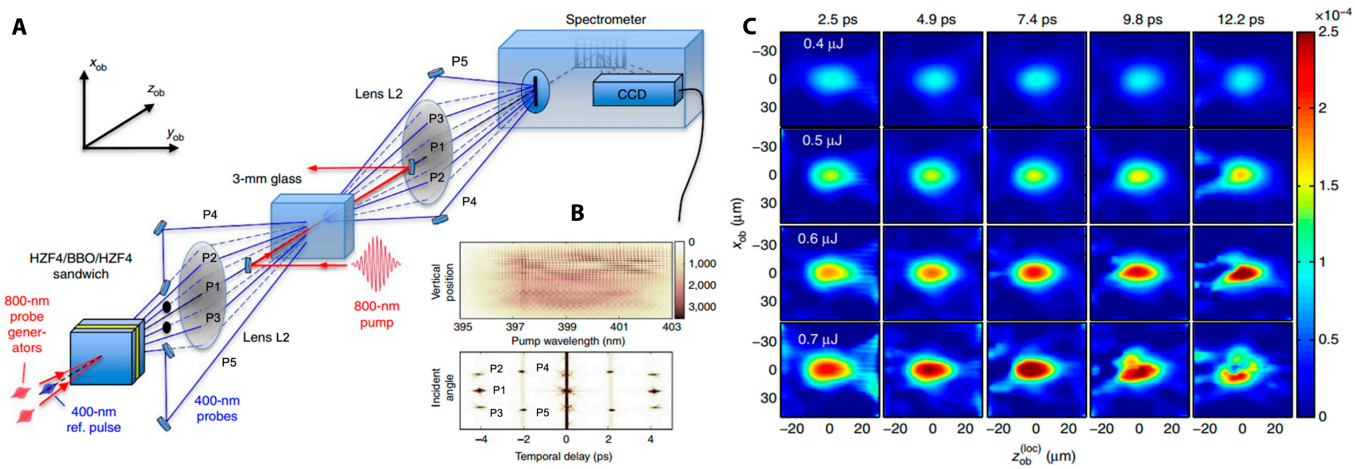

Fig. 14. The experimental setup of FDT (A), the 2D interferogram with the fringes in spectral and 1D spatial domains (B), and the selected 2D snapshots of the nonlinear refractive index profile at 5 propagating instants with different pump energy (C) [97].

photography" (CUST) [104] has realized its active detection by combining compressed sensing (CS) algorithm with time–wavelength coding instead of the original electro-optical scanning. CUST includes 3 parts: spectral-shaping module (see Fig. 15A), pulse-stretching module (see Fig. 15B), and compressed camera (see Fig. 15C). Spectral-shaping module is a traditional zero-dispersive system based on a pair of gratings (G1 and G2), a 4-*f* system (confocal lens pair of L_1 and L_2) with a slit at its Fourier plane, working to select a designated spectrum of the input femtosecond pulse. Pulse-stretching module is composed of another pair of gratings (G3 and G4), which stretches the probe pulse duration from some femtoseconds up to some picoseconds to cover the transient object. In the compressed camera, the probe beam carrying the target information passes firstly through an imaging lens (L3 in Fig. 15C). After projected on a digital micromirror device and encoded by a pseudo-random binary pattern, the probe is then imaged onto a camera by a 4-*f* imaging system (L4 and L5), where a grating (G5) is set at its Fourier plane to separate the different wavelength components of the probe at different spatial regions of the CCD. The transient scene is finally reconstructed by CS algorithm. Figure 15D shows the reflection process of pulse at the interface of Kerr medium (CS_2) by CUST with a frame interval of 414 fs and a frame number of 60, and the spectral

resolution is as fine as 0.25 nm. Accordingly, CUST can work with ultrahigh frame rate, large frame number, and high spectral resolution. In addition, its frame interval can be continuously tuned from 0.1 to 5 ps. However, increasing the frame number will inevitably sacrifice the temporal resolution (exposure time) due to CUST that is based on wavelength division. Similar to OPR [96], the recorded beam of CUST is dispersed spatially, which causes color smearing on the image plane, and, thus, degrades the spatial resolution.

Similar to CUST, chirped spectral mapping ultrafast photography (CSMUP) [39] also works with active detection mode via time–wavelength coding. There, the direct measured with the hyperspectral camera is a 2D (x, y) image but can be converted to a 3D dynamic scene (x–y–t) with simple reconstruction algorithm. As shown in Fig. 16A, the probe beam is a supercontinuum beam from visible to NIR, which is generated using an 800-nm femtosecond pulse to pump a YAG crystal. The supercontinuum is then chirped and stretched temporally to cover the transient event and realize time–wavelength coding after passing through the target event and finally recorded with a hyperspectral camera that collects 25 spectral images of different wavelengths from 659 to 949 nm. Figure 16B presents the filter arrangement on the CMOS sensor of the hyperspectral camera, while Fig. 16C exhibits the corresponding spectral responses of 25 bands. Because no movement occurs, the spatial resolution of CSMUP can be calibrated with a static target. Experimental results show that CSMUP can clearly see the features (228 lp/mm) of a 1951 USAF resolution pattern (Fig. 16D) and a grating of 1,200 lp/mm (Fig. 16E), which means that its spatial resolution is better than 833 nm. Targeting with the dynamical evolution of femtosecond laser ablation in silicon, CSMUP has taken 25-frame snapshots with a frame rate of ~0.25 Tfps (or a frame interval of 4 ps).

Despite that both CUST and CSMUP are based on time–wavelength coding, CSMUP has diffraction-limited spatial resolution due to the absence of the angular dispersion on the imaging plane. Moreover, CSMUP has a simpler and more compact configuration. However, the frame number of CSMUP depends on filter channels, which limits it to get large frame number.

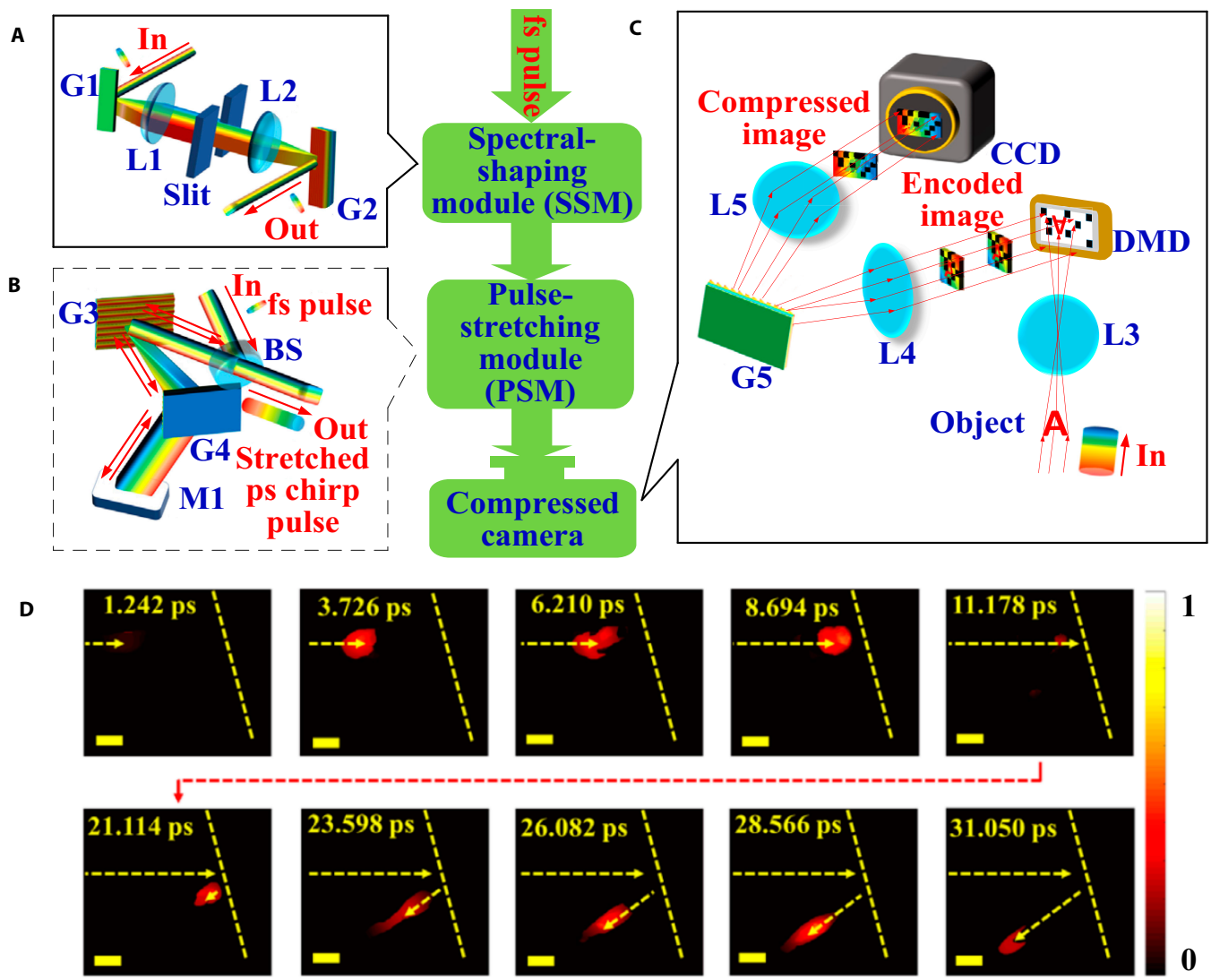

Fig. 15. Schematic diagram of CUST system: spectral-shaping module (A), pulse-stretching module (B), compressed camera (C), and the snapshots of a reflected light pulse (D) [104].

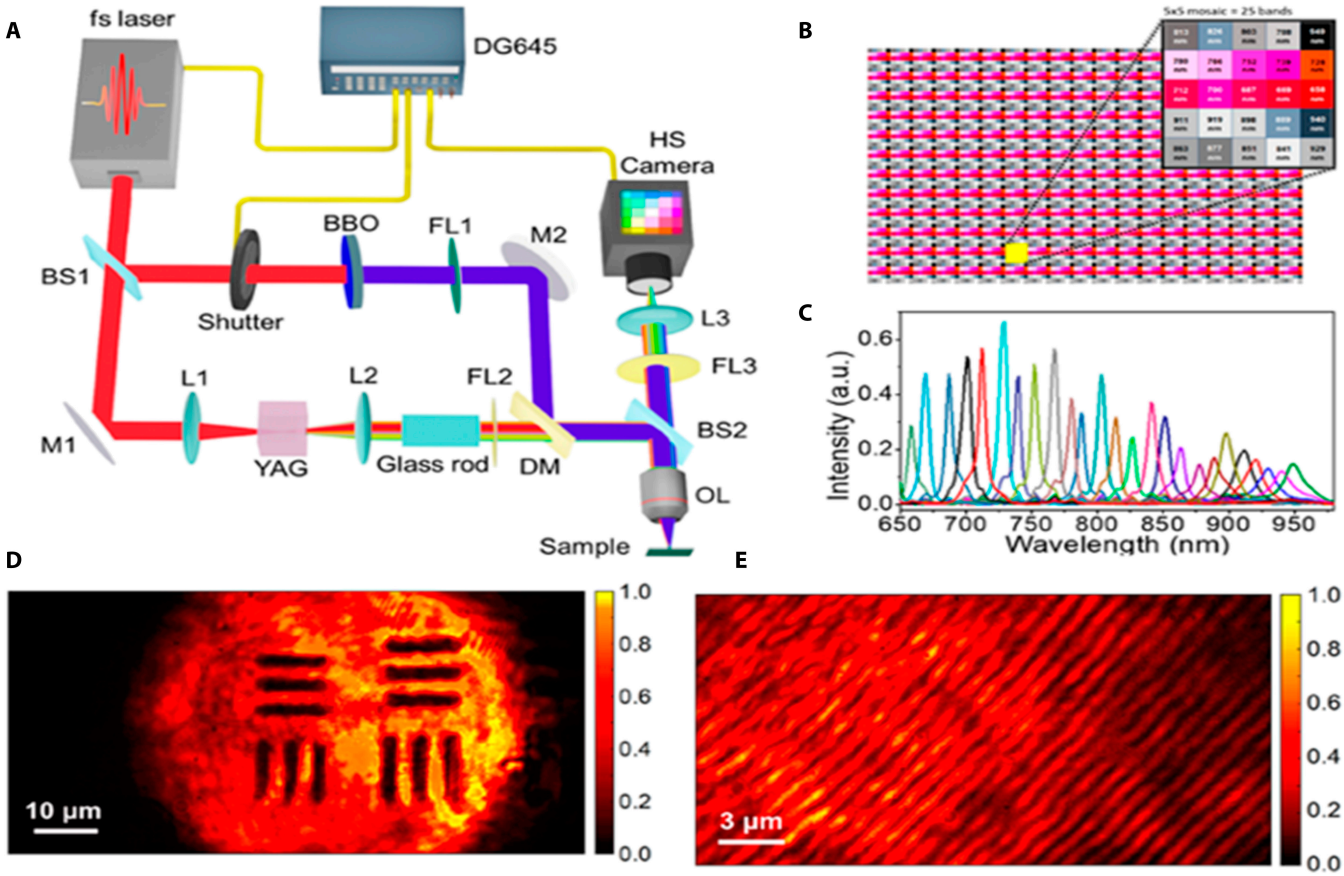

Fig. 16. Experimental layout of CSMUP for imaging the ultrashort pulse laser ablation (A), filter arrangement on the surface of CMOS sensor for hyperspectral imaging (B), 25-band spectral responses in the hyperspectral camera (C), images of the 1951 USAF resolution at 228 lp/mm (D), and a grating with 1,200 lp/mm (E) with CSMUP [39].

Polarization division

It is well known that polarization, one of the important degrees of a light field freedom, is usually manipulated and applied in many fields, including optical imaging. The strategy of time–polarization coding is to use polarization-sensitive optical elements to split the probe ultrafast pulse by orthogonal polarization components and make them have specified time delays to sample the target information at specified instants. Then, these polarization components are spatially separated and recorded by different detectors or different areas of the same detector to get the multiple-frame images. In 2013, Baker et al. [52] implemented time–polarization coding in a high-speed solid-state framing camera. By using 2D spatial profile of the flux incident on a cadmium selenide plate as target, the camera can realize 2-frame ultrafast imaging by a frame rate of 0.2 Tfps and a spatial resolution of 20 lp/mm. However, in this setup, the polarization multiplexing only supports 2 independent channels with orthogonal polarization states, which sets a barrier for further increase in the frame number.

Nevertheless, if working together with other coding methods, time–polarization coding can be used to double the frame number of SS-AUOI at least. For example, time–polarization coding and nonlinear double-frequency, 4-frame SS-AUOI [105] are available. By combining the time–polarization coding with time–wavelength coding, ultrafast all-optical solid-state framing camera (UASFC) [106] can promote the frame number from 2 to 6. Figure 17A and B exhibits the principle of UASFC. A femtosecond probe pulse with broad spectral bandwidth passes firstly through a time-series system, where a SF10 glass rod is used to temporally stretch the pulse for time–wavelength coding. A birefringent plate with a half-wave plate works to induce polarization-dependent time delay when the probe evolves into a pair of chirped pulses with orthogonal polarizations. These 2 pulses are then modulated by the target, a transient phase grating stemmed from an ultrafast semiconductor chip. After a 4-*f* spatial filter system, the 2 pulses carrying the target information are spatially manipulated to convert the phase modulation to amplitude modulation. Here, a spatial mapping device (SMD), including a beam displacer, 2 beam splitters, and 3 narrow band filters (F1 to F3), is applied to separate 2 groups of the polarization-orthogonal beams, each of which has 3 subbeams with 5-nm bandwidth and with central wavelengths at 790, 800, and 810 nm, separately. As a result, after SMD, these beams or the 6 frame images are imaged on different areas of a sensor. The frame rate is 0.33 Tfps, while the spatial resolution is 30 lp/mm.

SS-AUOI by Computational Imaging

Computational imaging opened a new paradigm of optics and information processing fields about 30 years ago. In the paradigm, a key feature is the miraculously joint design of optical system and signal processing after detection or the codesign of hardware and software to renovate the optical imaging [107]. Current investigations show that computational imaging can present "a global optimization method" [108], reduce the

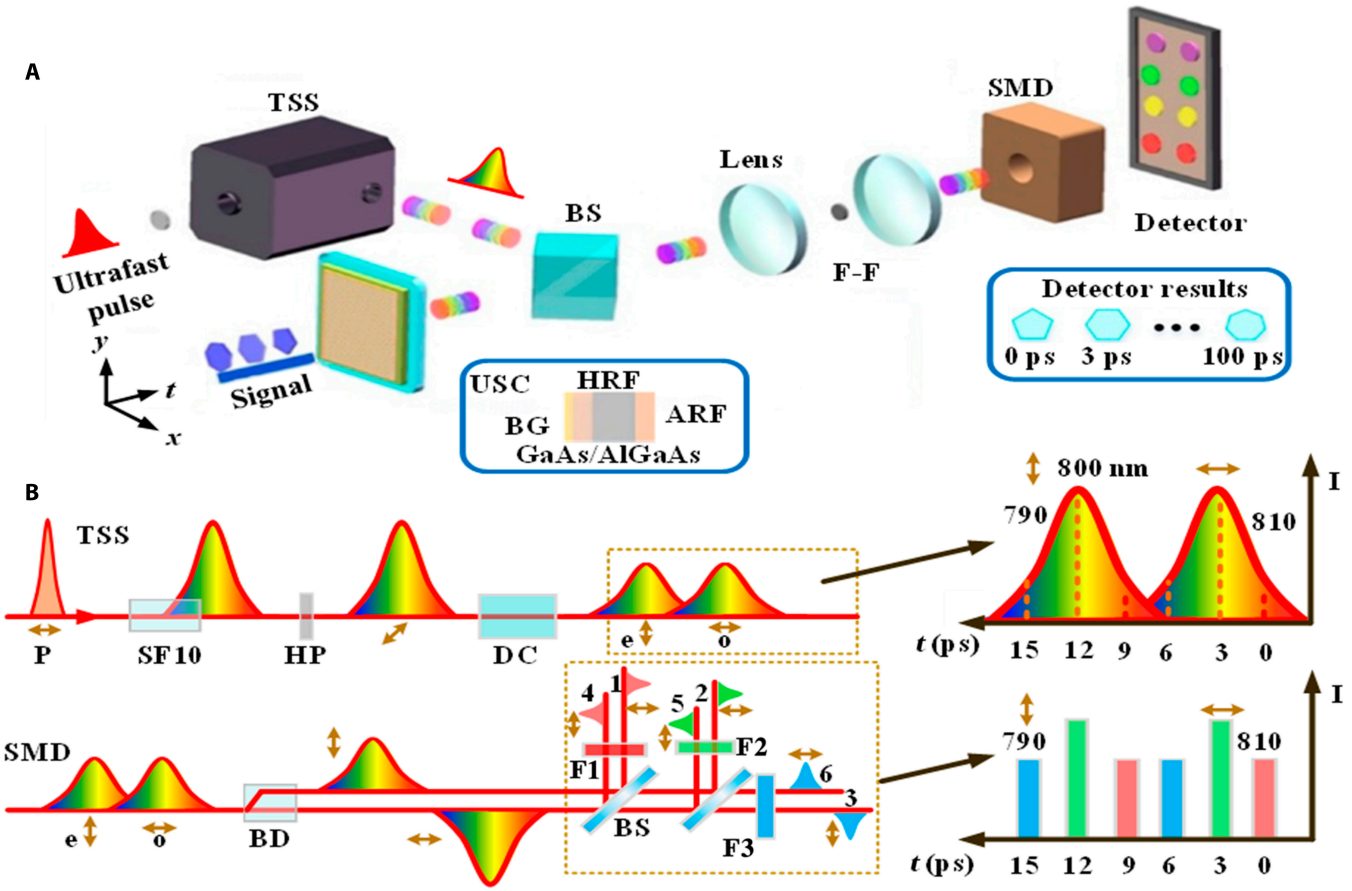

Fig. 17. Schematic diagrams of the UASFC (A), the time-series system (TSS) and the SMD. F-F, Fourier filter; USC, ultrafast semiconductor chip; BG, binary grating; HRF, high-reflection film; ARF, antireflection film; DC, delay crystal; BD, beam displacer; F1 to F3, filters (B) [106].

system complexity [109], and extend the system's capability [110,111]. Accordingly, merging the computational imaging to ultrafast imaging is very interesting but challenging.

Traditionally, optical imaging is carried out by recording directly the images or its Fourier spectra. However, the computational imaging systems just capture the optical fields implicitly carrying target information, so some special imaging algorithms are required to recover the imaging features. Until now, the typical computational imaging algorithms involved with SS-AUOI are coherent diffraction imaging (CDI) [55] (including ptychography [112]), CS [113], tomography [95,114], and so on.

CDI is a powerful imaging technique that is simple and easy to implement. It collects intensities of the diffraction wave and then uses iterative feedback algorithms to reconstruct an image [12]. It can reach diffraction-limited resolution via iterative reconstructions [54,115]. The outstanding advantage of CDI lies in its capability to realize phase imaging with simple optical alignment, and the accuracy and image quality are comparable to that of traditional interferometry and holography, even in the regime of visible region. Since its first experimental demonstration in 1999 [116], CDI has gained rapid development and becomes merged with single-shot ultrafast optical imaging. Correspondingly, some CDI algorithms [55,112,117] have been reported, which are integrated with single-shot ultrafast optical imaging.

Ptychography, one of the powerful CDI methods measures overlapped diffractive intensity of different parts of a test object and reconstructs the phase by iterative retrieval algorithms [118] with no need of the reference such as interferometry and holography. Up to now, many varieties of CDI algorithms (e.g., multimode CDI algorithm) [119–121] have been proposed to recover accurately complex-valued objects, and high spatial resolution [122] are available. However, traditional ptychography needs scanning [123], which prevents it from working for single-shot optical imaging. As a pioneering work, in 2013, Pan et al. [124] developed a single-shot ptychographic iterative engine by multi-illuminations with a transmission grating. In 2016, Sidorenko and Cohen [125] proposed single-shot ptychographic microscopes. By using this robust setup, an array of illuminating spots including tens or hundreds of partially overlapping intensity diffraction patterns was recorded with a single shot but short exposure, as well as high spatial resolution and a large FOV. Sooner or later, illuminated by a single 150-ps pulse, single-shot ultrafast ptychography [112] was demonstrated despite it using a static target. To produce a movie of the event from the recorded multiplexed ptychographic data, time-resolved imaging by multiplexed ptychography (TIMP) [117] was realized using a multistate ptychographic algorithm [121,126] to replace ordinary ptychographic reconstruction algorithm. As shown in Fig. 18A, TIMP includes a 4-*f* optical system and 2 SLMs. One SLM at the front focal plane of the 4-*f* system is used for multiple-position illumination, while the other one, after the lens with a little displacement from the Fourier plane, works to produce dynamic object and thereby

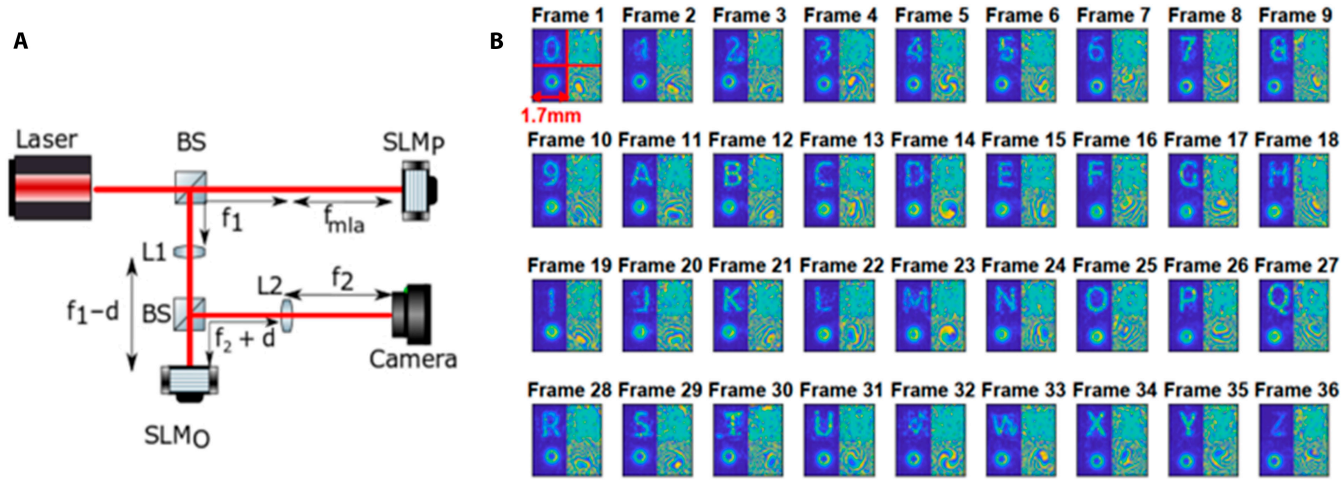

Fig. 18. Schematic setup of TIMP (A), the reconstructed frames of complex-valued objects and probed by 4 quarters of each frame (as marked on the first frame): top left, top right, bottom left, and bottom right for object amplitude and phase information, respectively (B) [117].

to create partial overlap between neighboring illumination beams. The different far-field diffraction patterns of objects from the corresponding illumination spots are then recorded with one camera. For single-shot imaging, orbital angular momentum coding (4 orbital angular momentum modes) and phase gradient coding (9 phase gradient modes) are chosen to produce mutually orthogonal pulse train for the capture of the ptychographic multiplexing information. As a result, 36 frames of a dynamical complex-valued object are obtained successfully, as shown in Fig. 18B. There, the spatial resolution is 300 μm, limited by the recording mode of spatial division, while the frame rate depends on the frame rate of the SLMs. However, in TIMP, both the spatial resolution and frame rate are largely independent of the frame number. Increasing the frame number can be realized by reducing the FOV or enhancing the complexity of the microscope [112]. Accordingly, TIMP may allow ultrahigh speed microscopy of complex-valued objects with a spatial scale of submicrometer and a temporal scale of picoseconds.

Recently, single-shot ultrafast multiplexed CDI (SUM-CDI) [54] was reported, which is implemented by the setup of Fig. 19A. There, the 355- and 532-nm *Q*-switch laser pulses are obtained from an 8-ns and 1,064-nm laser source via double- and triple-frequency conversions with 2 pieces of β-BBO crystals (BBO-1 and BBO-2). The 355-nm pulse illuminates a piece of K9 glass to generate laser-induced damage as the target. The 532-nm beam is split into 4 beamlets by a fiber coupler. Each of the beamlets delays by a single-mode fiber to form a temporal interval of 10 ns among them. Then, they are guided to parallelly illuminate the target by slightly different incident angles. Each of the beams is split further by a Dammann grating into 3×3 replicas and then passes through a random $0 - \pi$ binary phase plate to encode 4 overlapped diffraction patterns. The recorded intensity is the summation of 4 frames of diffraction intensities corresponding to 4 probe pulses. Obviously, in Fig. 19A, the laser probes illuminate the target in sequence, and the diffraction pattern arrays formed by each laser pulse are recorded at different instants with a single detector. On the basis of this design, 4-frame images, including both phase and amplitude information, can be iteratively retrieved with a high signal-to-noise ratio via the multiplex phase retrieval algorithm that combines ptychography with common coherent modulation imaging algorithm [127]. As shown in Fig. 19B and C, the performance of this scheme was verified by imaging the laser filament and shock wave during the occurrence and evolution of laser-induced damage inside K9 glass. The images have 10-ns temporal resolution and 6.96-μm spatial resolution. In SUM-CDI, the multiplexed algorithm can avoid the data division in spatial domain or frequency domain that is helpful to get high spatial resolution. The spatial resolution can be improved further with a larger sensor. The temporal resolution is limited by pulse duration of illuminating pulses, so it can be further improved using shorter laser pulse. However, the large dispersion induced by the fiber-based elements may make SUM-CDI fail to work well in femtosecond region.

In 2019, Hu and his co-workers [46] proposed another interesting design related to CDI, termed single-shot ultrafast phase retrieval photography (SUP). The setup just includes a multiplexed time-delay illumination chip, a 4-*f* optical system, and a CCD camera seeded with a femtosecond laser source (see Fig. 20A), so it is very simple and compact. As shown in Fig. 20B, the key component of SUP is a silicon photonic integrated chip, which works not only for multiangle illumination but also for ultrashort time delays for each illumination beam. SUP has combined the hybrid input–output algorithm with error reduction algorithm [128] so that it can recover both amplitude and phase of the image by measuring the diffraction pattern and enforcing iteratively a set of constraints, as shown in Fig. 20C. Experimentally, single-shot 16-frame ptychography was realized by a spatial resolution of <5 lp/mm and a frame rate of 1 Tfps with a static complex-valued target. The chip-based strategies significantly reduce the spatial complexity of the imaging system and can easily increase the number of frames. However, as SUP works by allocating a diffraction cone to each frame, increasing the frame number inherently decreases the spatial resolution.

CS algorithm [129] has drowned great attention in ultrafast imaging field since it was applied to ultrafast imaging. In CUP system, imaging information is encoded with a pseudo-random binary pattern and then maps its time variation to the space dimension with a streak camera. Accordingly, CUP can measure an *x*–*y*–*t* scene with a single camera snapshot. Finally, CS algorithm is used to process the recoded image data. The excellent combination of the hardware and algorithm allows CUP to

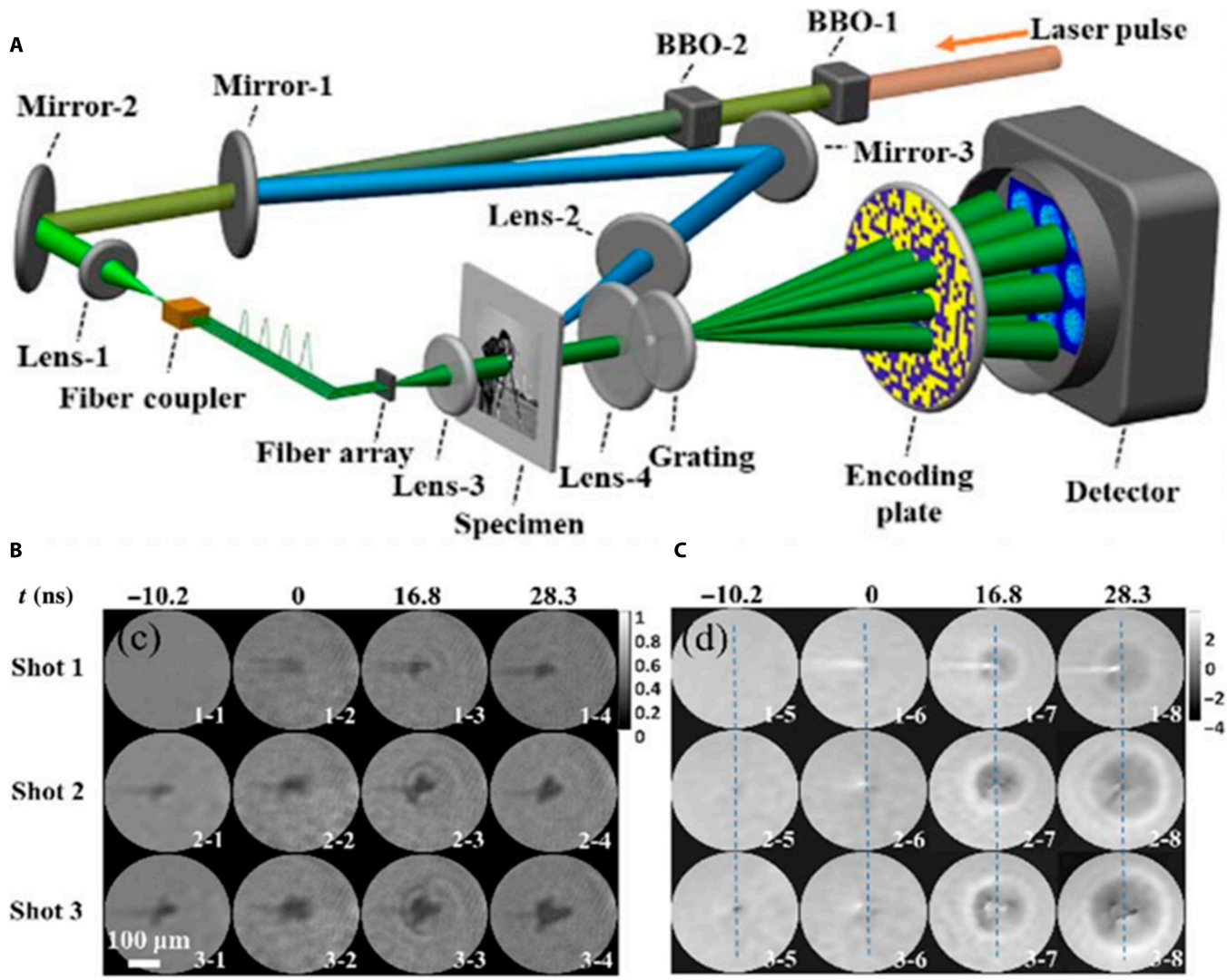

Fig. 19. Optical layout of SUM-CDI system (A), the amplitude (B), and phase (C) distributions at the corresponding moments of each frame reconstructed by SUM–CDI [54].

record highly compressible data and to reconstruct the sequential images with a temporal resolution of tens of picoseconds and a large frame number (beyond 1,000). Although the first CUP [26] operated with passive detection mode, active CUP technologies have gotten a rapid development in recent years. Extending the CS algorithms from the x–y–t data to the x–y–ω (x, y, spatial coordinates; ω, frequency), some all-optical CUP-based designs have been developed, e.g., CUST [104] and CSMUP [39]. Merging augmented Lagrangian and alternating direction algorithms into CS algorithm (TVAL3) [130] can not only reconstruct a rapidly moving light pulse with a more precise profile and more fitted trajectory but also promote the reconstruction speed. For CUP-based system, large frame number usually works with low image quality, thus poor ability to observe transient scenes with fine spatial features. This restriction was greatly alleviated by merging weighted multiscale denoising to the plug-and-play-based alternating direction method of multipliers framework [131] and thereby significantly improves the quality of image reconstruction. Another interesting CUP-based system worth to mention is "single-shot compressed optical field topography" (COFT) [132]. Algorithmically, COFT is based on a global 3D phase retrieval algorithm, which includes Gerchber–Saxton [122] algorithm and FROG evolutionary algorithm [133] used for spatial phase and spectral phase retrieval. This 3D algorithm allows COFT to recover an ultrafast optical field with both amplitude and phase information, which have not been resolved by traditional CUP-based system before.

Tomography, a cross-sectional imaging by detecting the radiation through an object along different directions, can be applied for non-line-of-sight imaging or noninvasive imaging of hidden stationary target. As early as 2014, Li et al. [97] adapted some established CT algorithms [134], for the first time to reconstruct ultrafast spatiotemporal dynamics in single-shot mode. There, the sagacious use of CT allows the implementation of the innovative but compact and inexpensive design: to generate the multiprobe array in a single step by cascaded 4-wave mixing and multiplex all probes to one spectrometer and extracted phase streaks in both space and time from the recorded hologram. This work opens a new way to 4-dimensionally visualize the propagation of a light velocity object in single-shot mode.

CT is the first one of the mathematical algorithms merging single-shot ultrafast imaging with non-line-of-sight imaging.

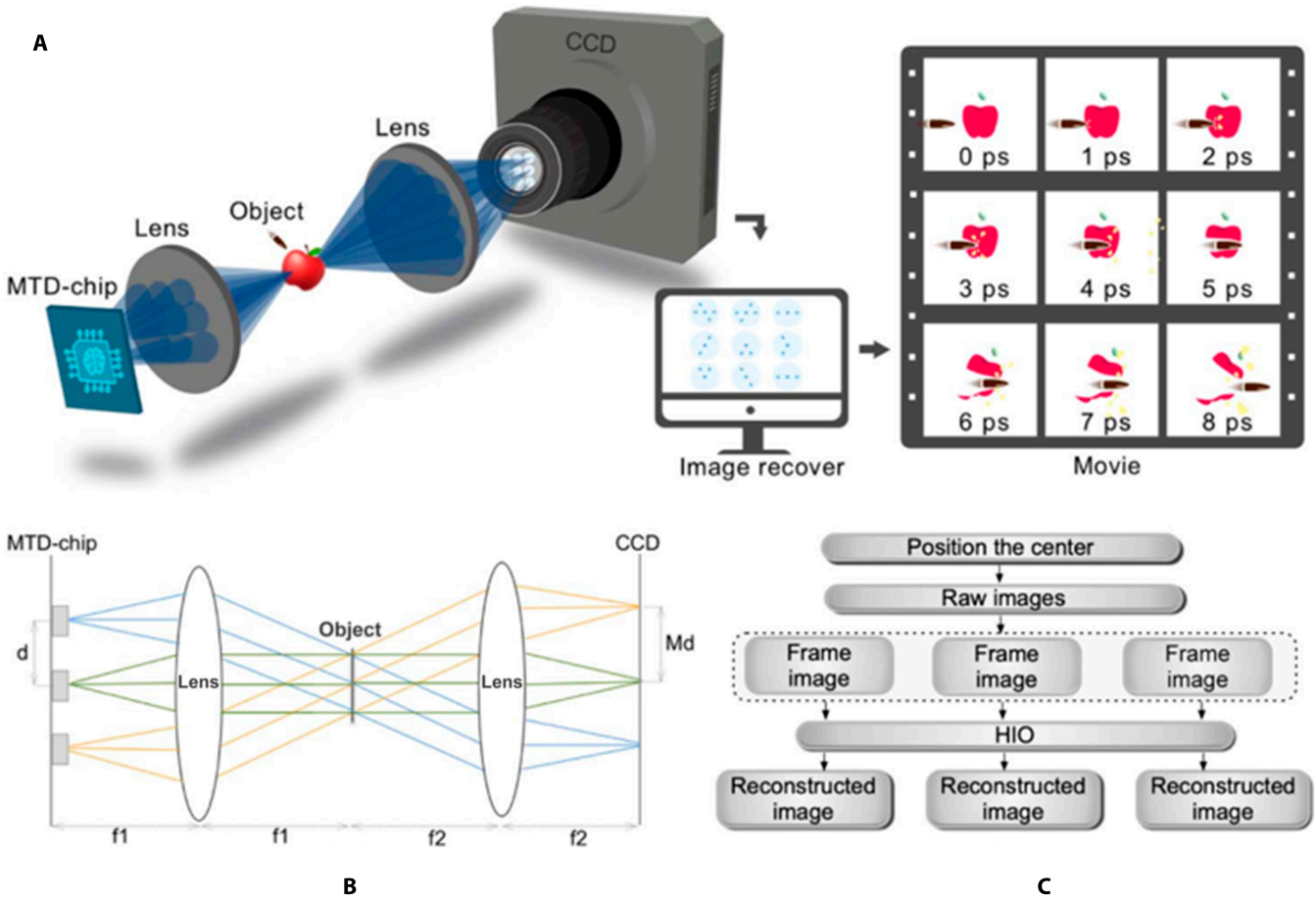

Fig. 20. Optical setup of SUP (A), its illustration of ray trajectory (B), and the hybrid input–output (HIO) algorithm-based iterative phase retrieval procedure (C) [46]. MTD-chip, multiplexed time-delay illumination chip.

This work was performed by Feng and Gao [101] with a design of ultrafast light field tomography (LIFT). LIFT is mathematically equivalent to CT using parallel beam projection plus a deep adjoint neural network to accelerate and improve LIFT image recovery by learning and mitigating the system's implementation limitations. Figure 21A illustrates the image formation by a cylindrical lens, while Fig. 21B shows the 2-step modeling of cylindrical lenslet imaging process. Figure 21C is the typical setup of an LIFT camera, and Fig. 21D presents a 3D space and time characterization of a picosecond laser pulse propagating inside a light-diffusing fiber captured by LIFT camera. Figure 21E is the time-integrated 3D image of the helical fiber. With LIFT, 3D imaging of light in flight phenomena with a <10-ps resolution was demonstrated experimentally. In addition, LIFT also showcases its non-line-of-sight imaging targeted with a hidden scene consisting of a static strip and one circular plate and recording the 2D time-resolved data with an exposure time of 10 ns. Although LIFT is an SS-PUOI, it can work as spectral domain LIFT [101] by active detection with sub-100-fs temporal resolution and 1,000 frames if a suitable laser source is equipped.

Prospect of SS-AUOI

In recent several decades, great progress has been made for SS-AUOI, featuring record-high imaging speeds, high temporal resolution, and large frame number. Up to date, SS-AUOI has achieved its resolved time to tens of femtoseconds [35], spatial resolution to subnanometers [14], frame rate up to 70 Tfps, and the frame number up to 1,000 [100]. Nevertheless, driven by many applications in a wide span of scientific and industrial fields, SS-AUOI is still a hot topic in many fields.

Undoubtedly, SS-AUOI will push its temporal resolution into femtosecond, even subfemtosecond or attosecond, region. With the development of femtosecond lasers, we believe that femtosecond resolution faces one of the main challenges from the dispersion management. For a sub-10-fs laser pulse, even passing through a very thin optical plate, the pulse duration will be stretched greatly, which will degrade the temporal resolution. Moreover, once the angular dispersion occurs, the strong dispersion also impairs the spatial resolution. Accordingly, the shorter pulse duration used, the greater trouble for the hardware design of SS-AUOI system.

Recently, with the advent of subfemtosecond laser sources [135], it is possible to achieve subfemtosecond or attosecond (10^{-18} s) temporal resolution. However, until now, the subfemtosecond sources almost operate in extreme ultraviolet or x-ray region, so the SS-AUOI needs totally fresh mechanism and faces a comprehensive challenge, but it is very interesting and exciting.

For the transient events with a time scale as short as some picoseconds, the temporal synchronization is critical between

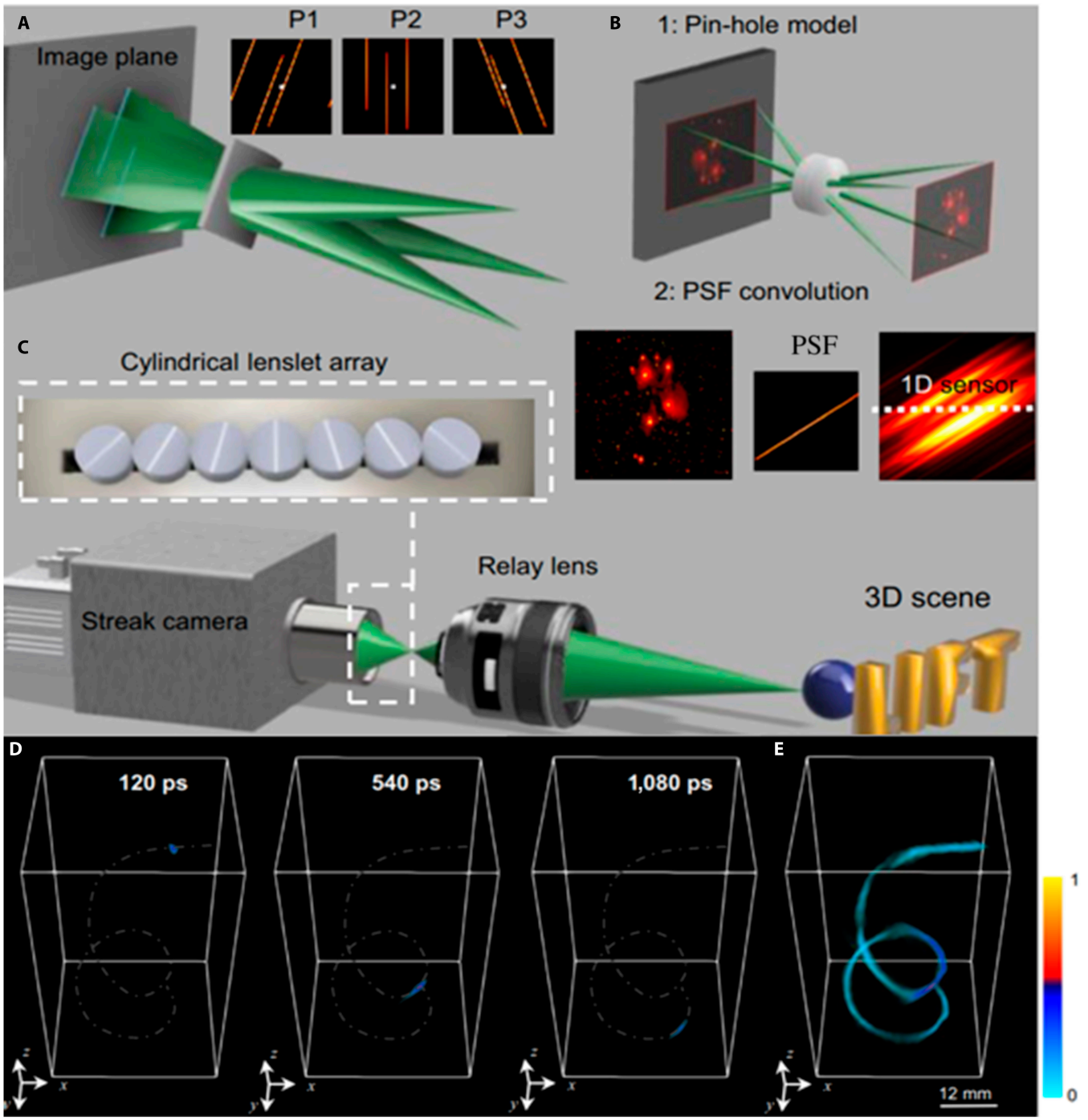

Fig. 21. Imaging process with a cylindrical lens (A), the 2-step imaging process modeling of cylindrical lenslet (B), typical layout of a LIFT camera (C), a 3D space plus time characterization of a picosecond laser pulse propagating inside a light-diffusing fiber (D), and time-integrated 3D image of the helical fiber (E) [101].

SS-AUOI system and the target, which may become main limitation of some SS-AUOI applications. Increasing the synchronous accuracy can loosen the requirement of frame number. The larger frame number, the lower synchronous accuracy needed. As it is known, one of the merits of the CS-based photographers is their large frame number. Unfortunately, the photographers usually relate the frame number with the spatial resolutions: the larger frame number means poorer spatial resolutions. Other SS-AUOI systems have never been reported their frame number more than 100. In the future, besides increasing the synchronous accuracy, developing SS-AUOI systems together with large frame number, high temporal and spatial resolutions are a critical task for the femtosecond to picosecond ultrafast targets.

Single-shot ultrafast phase imaging is also an active research topic. As we know, for the ultrafast events with picosecond or femtosecond scale, their features usually modulate the probe much weakly [136,137]. Phase imaging is usually more sensitive to the weak target information than the amplitude imaging and, thus, has superior imaging sensitivity. The SS-AUOI systems based on holography [54,75,80] can reconstruct target phases. However, the system designs for holographic interference make

them be bulky and unstable and prevent them from large frame number. CDI can help realizing SS-AUOI without the need of the interference arrangements, but, until now, the reported results [46,54,117] show that this work are facing great challenge in spatial/temporal resolutions, the frame rate, and the frame number. Integrating the dark-field imaging into the CUP system [138] has realized picosecond-resolution phase-sensitive imaging in single-shot mode, which, despite working with passive detection mode, has already ignited hope for the phase imaging of CUP-based SS-AUOI. In addition, vortex phase-contrast imaging based on, e.g., nonlinear frequency conversion [139–141], may also be a promising candidate for single-shot ultrafast phase imaging.

Single-shot ultrafast polarization imaging seems slow in coming. In 2020, Liang et al. [142] developed a stereo-polarimetric CUP (SP-CUP) to realize ultrafast polarization imaging of the early-stage plasma emission from laser-induced breakdown. SP-CUP works by passive detection, which means that single-shot active ultrafast polarization imaging has never been reported until now. However, we think that it is feasible to transform the SP-CUP into active detection mode, if necessary.

Developing SS-AUOI with high spatial resolution still has important demand pulls, such as laser nanofabrication and nanoprocessing [143,144], which need the spatial resolution at submicrometer or some nanometer level. With a probe at visible or NIR region, some imaging methods for super-resolution [145] shall be required to involved because of diffraction limit, which may be, e.g., synthesis sparse with analysis sparse [146], learning recurrent residual regressors [147], and some spatial frequency modulations [148,149]. In addition, using the probe with shorter wavelength is also helpful to promote the spatial resolution of SS-AUOI [150], which, however, may be limited by targets.

In recent years, some scientists have made their efforts to develop SS-AUOI with high-dimensional imaging. It is well known that different transient events have their own fingerprints apart from spatiotemporal information. For instance, multimode dissipative solitons evolve with transient spectral properties, and, correspondingly, spatiotemporal-spectral CS ultrafast photography [47] was created for 4D (2D spaces + time + spectrum) imaging with a rate up to trillions of frames per second. Similarly, spectral-volumetric CUP [151] was also invented for 4D imaging with submillimeter 2D spatial resolutions, 2-ps temporal frame interval, and 1.72-nm spectral frame interval. With the emerging application scenarios, high-dimensional SS-AUOI has very large developing space.

Extending SS-AUOI to wider spectral region deserves people's concern, too. Up to date, most of SS-AUOI systems work in visible or NIR region. In recent several decades, some frontier research fields, e.g., attosecond science [152,153], MIR laser [154,155], and terahertz radiation [156,157], have gotten great progresses. These progresses will inevitably push SS-AUOI toward extremely ultraviolet, x-ray region and, at the same time, to MIR and terahertz region, too.

In past decade, driven by many applications in a wide span of scientific fields, lots of advanced SS-AUOI systems have emerged, which have brought remarkable insights into various ultrafast phenomena. On the other hand, their application out of a laboratory environment is limited in most cases, either by the cost, complexity of the operation, or heavy data processing [93]. Accordingly, pushing SS-AUOI out of laboratory is also critical and non-negligible.

Conclusions

Compared with SS-PUOI, the SS-AUOI starts later but has its unique advantages. Using ultrafast laser pulses as the probe, SS-AUOI can flexibly implement some coding of its probe to extract sequential information without the need of any dynamical scanning, which opens a large space to get high frame rate and prevents the degradation of the spatial resolution (especially at high frame rate). However, the development of SS-AUOI is far from ideal until now. For time–space, time–spatial frequency, and time–polarization divisions, it is hard to get large frame number. Time–spectral coding can improve the dilemma, but its large frame number usually sacrifices its temporal resolution, which limits the effective frame rate. Computational imaging brings tremendous expectation of SS-AUOI, but it is still in infancy. In the future, the development of SS-AUOI will continue to be driven by 2 aspects. One is from the inner factor. For example, the emergence of novel coding may lead break, which can be expected from deeper intervention of computational imaging. Here, artificial intelligence [158] and deep learning [159,160] are worth looking forward to. New optical functional materials [161], elements, or devices can promote the SS-AUOI performance and ability, e.g., novel pulse shaper [162,163], splitter, and combiner [164,165]. In addition, novel coding methods realizing time–spatial separation more effectively may also be a yearning of the SS-AUOI developers. The other is demand pulls, which are always very important for any research fields, not excepting SS-AUOI. As discussed above, the demands are from physics to biomedicine engineering, from science to industrial fabrication, and from visible, NIR to MIR, or extremely ultraviolet region. Here, we would like to claim that we are unable to include all demands. Anyway, the research on SS-AUOI shows no sign of slowing down, and we do not think that it should slow down.

Acknowledgment

Funding: This work is partially supported by National Natural Science Foundation of China (92050203, 62075138, 62275163, and 12174264), Natural Science Foundation of Guangdong Province (2021A1515011909 and 2022A151501 1457), and Shenzhen Fundamental Research Program (JCYJ20 200109105606426, JCYJ20190808164007485, JCYJ2021 0324095213037, JCYJ-20190808121817100, JCYJ20190 808143419622, JSGG-20191231144201722, and JCYJ20190808115601653). **Author contributions:** X.Z. and X.L. were responsible for the parts of technical development and prospect of SS-AUOI, while Y.C. and S.X. were in charge of the parts including the introduction, characteristics of SS-AUOI, conclusions, and formal analysis. S.X. also provided the conceptualization and organization. S.X., X.Z., Y.C., and X.L. discussed the results. C.W., K.W., H.Z., Q.L., J.L., and R.Y. took part in preparing paper materials. All the authors took part in the preparation of the manuscript and reviewed the manuscript. All authors have read and agreed to the published version of the manuscript. **Competing interests:** The authors declare that they have no competing interests.

Data Availability

Correspondence and requests for materials should be addressed to S.X. or Y.C.

References

1. Mareev E, Pushkin A, Migal E, Lvov K, Stremoukhov S, Potemkin F. Single-shot femtosecond bulk micromachining of silicon with mid-IR tightly focused beams. *Sci Rep*. 2022;12:7517.
2. Betti R, Hurricane OA. Inertial-confinement fusion with lasers. *Nat Phys*. 2016;12:435.
3. Solli DR, Ropers C, Koonath P, Jalali B. Optical rogue waves. *Nature*. 2007;450:1054–1057.
4. Hockett P, Bisgaard C, Clarkin O, Stolow A. Time resolved imaging of purely valence electron dynamics during a chemical reaction. *Nat Phys*. 2011;7:612–615.
5. Wong C, Alvey R, Turner D, Wilk KE, Bryant DA, Curmi PMG, Silbey RJ, Scholes GD. Eletronic coherence lineshapes reveal hidden excitonic correlations in photosynthetic light harvesting. *Nat Chem*. 2012;4(5):396–404.
6. Herink G, Kurtz F, Jalali B, Solli DR, Ropers C. Real-time spectral interferometry probes the internal dynamics of femtosecond soliton molecules. *Science*. 2017;356:50–54.
7. Wang D, Wei S, Yuan X, Liu Z, Weng Y, Zhou Y, Xiao T, Goda K, Liu S, Lei C. Ultrafast imaging for uncovering laser–material interaction dynamics. *Int J Mech Syst Dyn*. 2022;2(1):65–81.
8. Deng X, Chao A, Feikes J, Hoehl A, Huang W, Klein R, Kruschinski A, Li J, Matveenko A, Petenev Y, et al. Experimental demonstration of the mechanism of steady-state microbunching. *Nature*. 2021;590:576–579.
9. Chen H. Toward unlimited temporal resolution: Femtosecond videography for atomic and molecular dynamics. *Light Sci Appl*. 2017;6:e17123.
10. Thompson JV, Bixler JN, Hokr BH, Noojin GD, Scully MO, Yakovlev VV. Single-shot chemical detection and identification with compressed hyperspectral Raman imaging. *Opt Lett*. 2017;42:2169.
11. Zewail AH. Femtochemistry: Atomic-scale dynamics of the chemical bond. *J Phys Chem A*. 2000;104:5660–5694.
12. Suzuki T, Hida R, Yamaguchi Y, Nakagawa K, Saiki T, Kannari F. Single-shot 25-frame burst imaging of ultrafast phase transition of $Ge_2Sb_2Te_5$ with a sub-picosecond resolution. *Appl Phys Express*. 2017;10:092502.
13. Dempsey D, Nagar GC, Renskers CK, Grynko RI, Sutherland JS, Shim B. Single-shot ultrafast visualization and measurement of laser–matter interactions in flexible glass using frequency domain holography. *Opt Lett*. 2020;45:1252.
14. Itina TE, Zakoldaev RA, Sergeev MM, Ma HF, Kudryashov SI, Medvedev OS, Veiko VP. Ultra-short laser-induced high aspect ratio densification in porous glass. *Opt Mater Express*. 2019;9:4379–4389.
15. Mareev EI, Rumiantsev BV, Migal EA, Bychkov AS, Karabutov AA, Cherepetskaya EB, Makarov VA, Potemki FV. A comprehensive approach to the characterization of the deposited energy density during laser–matter interactions in liquids and solid Meas. *Sci Technol*. 2020;31:085204.
16. Malinauskas M, Žukauskas A, Hasegawa S, Hayasaki Y, Mizeikis V, Buividas R, Juodkazis S. Ultrafast laser processing of materials: From science to industry. *Light Sci Appl*. 2016;5:e16133.
17. Fieramonti L, Bassi A, Foglia EA, Pistocchi A, D'Andrea C, Valentini G, Cubeddu R, De Silvestri S, Cerullo G, Cotelli F. Time-gated optical projection tomography allows visualization of adult zebrafish internal structures. *PLOS ONE*. 2012;7:e50744.
18. Chenu A, Scholes GD. Coherence in energy transfer and photosynthesis. *Annu Rev Phys Chem*. 2015;66:69–96.
19. Fuller PWW. An introduction to high-speed photography and photonics. *Imaging Sci J*. 2009;57(6):293–302.
20. Velten A, Willwacher T, Gupta O, Veeraraghavan A, Bawendi MG, Raskar R. Recovering three-dimensional shape around a corner using ultrafast time-of-flight imaging. *Nat Commun*. 2012;3:745.
21. Zewail AH. Four-dimensional electron microscopy. *Science*. 2010;328:187–193.
22. Suret P, Koussaifi R, Tikan A, Evain C, Randoux S, Szwaj C, Bielawski S. Single-shot observation of optical rogue waves in integrable turbulence using time microscopy. *Nat Commun*. 2016;7:13136.
23. Poulin PR, Nelson KA. Irreversible organic crystalline chemistry monitored in real time. *Science*. 2006;313:1756.
24. Ledingham KWD, McKenna P, Singhal RP. Applications for nuclear phenomena generated by ultra-intense lasers. *Science*. 2003;300(5622):1107–1111.
25. Liang J, Wang LV. Single-shot ultrafast optical imaging. *Optica*. 2018;5(9):1113–1127.
26. Gao L, Liang J, Li C, Wang LV. Single-shot compressed ultrafast photography at one hundred billion frames per second. *Nature*. 2014;516:74–77.
27. Liu X, Liu J, Jiang C, Vetrone F, Liang J. Single-shot compressed optical-streaking ultra-high-speed photography. *Opt Lett*. 2019;44:1387–1390.
28. Boyle WS, Smith GE. Charge coupled semiconductor devices. *Bell Syst Tech J*. 1970;49:587–593.
29. Kakue T, Tosa K, Yuasa J, Tahara T, Awatsuji Y, Nishio K, Ura S, Kubota T. Digital light-in-flight recording by holography by use of a femtosecond pulsed laser. *IEEE J Sel Top Quantum Electron*. 2012;18:479–485.
30. Wong TTW, Lau AKS, Ho KKY, Tang MYH, Joseph DF, Robles XW, Chan ACS, Tang AHL, Lam EY, Wong KKY, et al. Asymmetric-detection time-stretch optical microscopy (ATOM) for ultrafast high-contrast cellular imaging in flow. *Sci Rep*. 2014;4:3656.
31. Wakeham GP, Nelson KA. Dual-echelon single-shot femtosecond spectroscopy. *Opt Lett*. 2000;25:505–507.
32. Yue Q, Cheng Z, Han L, Yang Y, Guo C. One-shot time-resolved holographic polarization microscopy for imaging laser induced ultrafast phenomena. *Opt Express*. 2017;25:14182–14191.
33. Zeng X, Zheng S, Cai Y, Lin Q, Liang J, Lu X, Li J, Xie W, Xu S. High-spatial-resolution ultrafast framing imaging at 15 trillion frames per second by optical parametric amplification. *Adv. Photonics*. 2020;2(5):056002.
34. Tamburini F, Anzolin G, Umbriaco G, Bianchini A, Barbieri C. Overcoming the Rayleigh criterion limit with optical vortices. *Phys Rev Lett*. 2006;97:163903.
35. Offroy M, Roggo Y, Milanfar P, Duponchel L. Infrared chemical imaging: Spatial resolution evaluation and super-resolution concept. *Anal Chim Acta*. 2010;674:220.
36. Zhang K, Hu J, Yang W. Deep compressed imaging via optimized pattern scanning. *Photonics Res*. 2021;9:B57–B70.
37. Lei X, Shahid H, Wu S. A novel algorithm to improve image reconstruction quality for 2D streak camera. *Nucl Instrum Methods Phys Res A*. 2021;991:165023.

38. Mikami H, Gao L, Goda K. Ultrafast optical imaging technology: Principles and applications of emerging methods. *Nanophotonics*. 2016;5:497–509.
39. Ding P, Jin C, Wu X, Deng L, Jia T, Huang F, Liang J, Sun Z, Zhang S. Single-shot real-time ultrafast imaging of femtosecond laser fabrication. *ACS Photonics*. 2021;8:738–744.
40. Rulliere C. *Femtosecond laser pulses principles and experiments*Springer Science; 2005.
41. Zeng X, Zheng S, Cai Y, Wang H, Lu X, Wang H, Li J, Xie W, Xu S. Generation and imaging of a tunable ultrafast intensity-rotating optical field. *High Power Laser Sci Eng*. 2020;8:e3.
42. Wang X, Yan L, Si J, Matsuo S, Xu H, Hou X. High-frame-rate observation of single femtosecond laser pulse propagation in fused silica using an echelon and optical polarigraphy technique. *Appl Opt*. 2014;53:8395–8399.
43. Shin T, Wolfson J, Teitelbaum S, Kandyla M, Nelson K. Dual echelon femtosecond single-shot spectroscopy. *Rev Sci Instrum*. 2014;85:083115.
44. Li Z, Zgadzaj R, Wang X, Reed S, Dong P, Downer MC. Frequency-domain streak camera for ultrafast imaging of evolving light-velocity objects. *Opt Lett*. 2010;35:4087–4089.
45. Matlis N, Reed S, Bulanov S, Chvykov V, Kalintchenko G, Matsuoka T, Rousseau P, Yanovsky V, Maksimchuk A, Kalmykov S, et al. Snapshots of laser wakefields. *Nat Phys*. 2006;2:749–753.
46. Hu C, Du Z, Chen M, Yang S, Chen H. Single-shot ultrafast phase retrieval photography. *Opt Lett*. 2019;44:4419–4422.
47. Jing JC, Wei X, Wang LV. Spatio-temporal-spectral imaging of non-repeatable dissipative soliton dynamics. *Nat Commun*. 2020;11:2059.
48. Suzuki T, Isa F, Fujii L, Hirosawa K, Nakagawa K, Goda K, Sakuma I, Kannari F. Sequentially timed all-optical mapping photography (STAMP) utilizing spectral filtering. *Opt Express*. 2015;23:30512–30522.
49. Gao G, Tian J, Wang T, He K, Zhang C, Zhang J, Chen S, Jia H, Yuan F, Liang L, et al. Ultrafast all-optical imaging technique using low-temperature grown GaAs/$Al_xGa_{1-x}As$ multiple-quantum-well semiconductor. *Phys Lett*. 2017;381:3594–3598.
50. Liang J. Punching holes in light: Recent progress in single-shot coded-aperture optical imaging. *Rep Prog Phys*. 2020;83:116101.
51. Ehn A, Bood J, Li Z, Berrocal E, Aldén M, Kristensson E. FRAME: Femtosecond videography for atomic and molecular dynamics. *Light Sci Appl*. 2017;6:e17045.
52. Baker KL, Stewart RE, Steele PT, Vernon SP, Hsing WW, Remington BA. Solid-state framing camera with multiple time frames. *Appl Phys Lett*. 2013;103:151111.
53. Barolak J, Goldberger D, Squier J, Bellouard Y, Durfee C, Adams D. Wavelength-multiplexed single-shot ptychography. *Ultramicroscopy*. 2022;233:113418.
54. Xu YM, Pan XC, Sun MY, Liu WF, Liu C, Zhu JQ. Single-shot ultrafast multiplexed coherent diffraction imaging. *Photonics Res*. 2022;10:1937–1946.
55. Davis WC. A high-speed rotating-mirror framing camera. *Appl Opt*. 1962;1:407.
56. Racca RG, Dewey JM. High speed time-resolved holographic interferometer using solid-state shutters. *Opt Laser Technol*. 1990;22:199–204.
57. Chen GH, Li JF, Peng QX, Liu SX, Liu J. All-optical coaxial framing photography using parallel coherence shutters. *Opt Lett*. 2017;42:415–418.
58. Abramson N. Light-in-flight recording by holography. *Opt Lett*. 1978;3:121–123.
59. Kubota T, Komai K, Yamagiwa M, Awatsuji Y. Moving picture recording and observation of three-dimensional image of femtosecond light pulse propagation. *Opt Express*. 2007;15:14348–14354.
60. Rabal H, Pomarico J, Arizaga R. Light-in-flight digital holography display. *Appl Opt*. 1994;33:4358–4360.
61. Faccio D, Velten A. A trillion frames per second: The techniques and applications of light-in-flight photography. *Rep Prog Phys*. 2018;81:105901.
62. Sawashima Y, Yamanaka D, Takamoto I, Matsunaka A, Awatsuji Y, Nishio K. Extending recordable time of light-in-flight recording by holography with double reference light pulses. *Opt Lett*. 2018;43:5146–5149.
63. Sasaki M, Matsunaka A, Inoue T, Nishio K, Awatsuji Y. Motion-picture recording of ultrafast behavior of polarized light incident at Brewster's angle. *Sci Rep*. 2020;10(1):7638.
64. Hinrichs H, Hinsch KD, Kickstein J, Böhmer M. Light-in-flight holography for visualization and velocimetry in three-dimensional flows. *Opt Lett*. 1997;22:828–830.
65. Sven FH, Klaus DH. Light-in-flight holographic particle image velocimetry for wind-tunnel applications. *Meas Sci Technol*. 2004;15(4):613.
66. Fujimoto M, Aoshima S, Tsuchiya Y. Multiframe observation of an intense femtosecond optical pulse propagating in air. *Opt Lett*. 2002;27:309–311.
67. Yan L, Wang X, Si J, Matsuo S, Chen T, Tan W, Chen F, Hou X. Time-resolved single-shot imaging of femtosecond laser induced filaments using supercontinuum and optical polarigraphy. *Appl Phys Lett*. 2012;100:111107.
68. Huang K, Fang J, Yan M, Wu E, Zeng H. Wide-field mid-infrared single-photon upconversion imaging. *Nat Commun*. 2022;13(1):1077.
69. Huang K, Wang Y, Fang J, Kang W, Sun Y, Liang Y, Hao Q, Yan M, Zeng H. Mid-infrared photon counting and resolving via efficient frequency up-conversion. *Photonics Res*. 2021;9(2):259–265.
70. Scott RHH, Glize K, Antonelli L, Khan M, Theobald W, Wei M, Betti R, Stoeckl C, Seaton AG, Arber TD, et al. Shock ignition laser-plasma interactions in ignition-scale plasmas. *Phys Rev Lett*. 2021;127:065001.
71. Lei S, Zhao X, Yu X, Hu A, Vukelic S, Jun MBG, Joe H, Yao YL, Shin YC. Ultrafast laser applications in manufacturing processes: A state-of-the-art review. *ASME J Manuf Sci Eng*. 2020;142(3):031005.
72. Yan L, Wang X, Si J, He P, Chen F, Zou J, Hou X. Multi-frame observation of a single femtosecond laser pulse propagation using an echelon and optical polarigraphy technique. *IEEE Photonics Tech Lett*. 2013;25:1879–1881.
73. Wang X, Zhai H, Mu G. Pulsed digital holography system recording ultrafast process of the femtosecond order. *Opt Lett*. 2006;31:1636–1638.
74. Yeola S, Kuk D, Kim K-Y. Single-shot ultrafast imaging via spatiotemporal division of femtosecond laser pulses. *J Opt Soc Am B*. 2018;35:2822–2827.
75. Huang HY, Guo CS. Simple system for realizing single-shot ultrafast sequential imaging based on spatial multiplexing in-line holography. *Opt Express*. 2022;30(23):41613–41623.
76. Sheinman M, Erramilli S, Ziegler L, Hong MK, Mertz J. Flatfield ultrafast imaging with single-shot non-synchronous array photography. *Opt Lett*. 2022;47:577.

77. Zhu Q, Cai Y, Zeng X, Long H, Chen H, Zeng L, Zhu Y, Lu X, Li J. FISI: Frequency domain integration sequential imaging at 1.26×10^{13} frames per second and 108 lines per millimeter. *Opt Express*. 2022;30:27429–27438.
78. Zhang N, Zhu XN, Yang JJ, Wang XL, Wang MW. Time-resolved shadowgraphs of material ejection in intense femtosecond laser ablation of aluminum. *Phys Rev Lett*. 2007;99:167602–167604.
79. Moon J, Yoon S, Lim Y-S, Choi W. Single-shot imaging of microscopic dynamic scenes at 5 THz frame rates by time and spatial frequency multiplexing. *Opt Express*. 2020;28:4463.
80. Huang HY, Cheng ZJ, Yang Y, Yue QY, Guo CS. Single-shot ultrafast sequential holographic imaging with high temporal resolution and a large field of view. *Opt Lett*. 2019;44:4885.
81. Liu Z, Centurion M, Panotopoulos G, Hong J, Psaltis D. Holographic recording of fast events on a CCD camera. *Opt Lett*. 2002;27:22–24.
82. Sánchez-Ortiga E, Doblas A, Saavedra G, Martínez-Corral M, Garcia-Sucerquia J. Off-axis digital holographic microscopy: Practical design parameters for operating at diffraction limit. *Appl Opt*. 2014;53:2058.
83. Zhang C, Xu YQ, Wei XM, Tsia KK, Wong KKY. Time-stretch microscopy based on time-wavelength sequence reconstruction from wideband incoherent source. *Appl Phys Lett*. 2014;105:041113.
84. Cai Y, Chen ZK, Zeng XK, Shangguan HC, Lu XW, Song QY, Ai YX, Xu SX, Li JZ. The development of the temporal measurements for ultrashort laser pulses. *Appl Sci*. 2020;10:7401–7414.
85. Kalashnikov MP, Risse E, Schönnagel H, Sandner W. Double chirped-pulse-amplification laser: A way to clean pulses temporally. *Opt Lett*. 2005;30:923–925.
86. Kojima J, Nguyen Q-V. Laser pulse-stretching with multiple optical ring cavities. *Appl Opt*. 2002;41:6360.
87. Nakagawa K, Iwasaki A, Oishi Y, Horisaki R, Tsukamoto A, Nakamura A, Hirosawa K, Liao H, Ushida T, Goda K, et al. Sequentially timed all-optical mapping photography (STAMP). *Nat Photonics*. 2014;8:695–700.
88. Tamamitsu M, Nakagawa K, Horisaki R, Iwasaki A, Oishi Y, Tsukamoto A, Kannari F, Sakuma I, Goda K. Design for sequentially timed all-optical mapping photography with optimum temporal performance. *Opt Lett*. 2015;40(4):633–636.
89. Nemoto H, Suzuki T, Kannari F. Single-shot ultrafast burst imaging using an integral field spectroscope with a microlens array. *Opt Lett*. 2020;45:5004.
90. Saiki T, Hosobata T, Kono Y, Takeda M, Ishijima A, Tamamitsu M, Kitagawa Y, Goda K, Morita SY, Ozaki S, et al. Sequentially timed all-optical mapping photography boosted by a branched 4f system with a slicing mirror. *Opt Express*. 2020;28(21):31914–31922.
91. Yuan X, Li Z, Zhou J, Liu S, Wang D, Lei C. Hybrid-plane spectrum slicing for sequentially timed all-optical mapping photography. *Opt Lett*. 2022;47(18):4822.
92. Touil M, Idlahcen S, Becheker R, Lebrun D, Rozé C, Hideur A, Godin T. Acousto-optically driven lensless single-shot ultrafast optical imaging. *Light Sci Appl*. 2022;11:66.
93. Nemoto H, Suzuki T, Kannari F. Extension of time window into nanoseconds in single-shot ultrafast burst imaging by spectrally sweeping pulses. *Appl Opt*. 2020;59:5210–5215.
94. Wu JL, Xu YQ, Xu JJ, Wei XM, Chan AC, Tang AH, Lau AK, Chung BM, Shum HC, Lam EY, et al. Ultrafast laser-scanning time-stretch imaging at visible wavelengths. *Light Sci Appl*. 2017;6:e16196.
95. Xu YQ, Murdoch SG. Real-time spectral analysis of ultrafast pulses using a free-space angular chirp-enhanced delay. *Opt Lett*. 2019;44:3697–3700.
96. Zhu Y, Zeng X, Cai Y, Lu X, Zhu Q, Zeng L, He T, Li J, Yang Y, Zheng M, et al. All-optical high spatial-temporal resolution photography with raster principle at 2 trillion frames per second. *Opt Express*. 2021;29(17):27298–27308.
97. Li Z, Zgadzaj R, Wang X, Chang Y-Y, Downer MC. Single-shot tomographic movies of evolving light-velocity objects. *Nat Commun*. 2014;5:3085.
98. Gibson GM, Johnson SD, Padgett MJ. Single-pixel imaging 12 years on: A review. *Opt Express*. 2020;28:28190–28208.
99. Yuan X, Brady DJ, Katsaggelos AK. Snapshot compressive imaging: Theory, algorithms, and applications. *IEEE Signal Process Mag*. 2021;38:65–88.
100. Wang P, Liang J, Wang L. Single-shot ultrafast imaging attaining 70 trillion frames per second. *Nat Commun*. 2020;11:2091.
101. Feng X, Gao L. Ultrafast light field tomography for snapshot transient and non-line-of-sight imaging. *Nat Commun*. 2021;12:2179.
102. Satat G, Tancik M, Raskar R. Lensless imaging with compressive ultrafast sensing. *IEEE Trans Comput Imaging*. 2017;3:398–407.
103. Yang C, Qi D, Cao F, He Y, Yao J, Ding P, Ouyang X, Yu Y, Jia T, Xu S, et al. Single-shot receive-only ultrafast electro-optical deflection imaging. *Phys Rev Appl*. 2020;13:024001.
104. Lu Y, Wong TW, Chen F, Wang L. Compressed ultrafast spectral-temporal photograpy. *Phys Rev Lett*. 2019;122:193904.
105. Davidson ZE, Gonzalez-Izquierdo B, Higginson A, Lancaster KL, Williamson SDR, King M, Farley D, Neely D, McKenna P, Gray RJ. An optically multiplexed single-shot time-resolved probe of laser–plasma dynamics. *Opt Express*. 2019;27:4416–4423.
106. Gao G, He K, Tian J, Zhang C, Zhang J, Wang T, Chen S, Jia H, Yuan F, Liang L, et al. Ultrafast all-optical solid-state framing camera with picosecond temporal resolution. *Opt Express*. 2017;25(8):8721–8729.
107. Mait JN, Euliss GW, Athale RA. Computational imaging. *Adv Opt Photon*. 2018;10:409–483.
108. Li JY, Zhao L, Wu XQ, Liu F, Wei YZ, Yu C, Shao XP. Computational optical system design: A global optimization method in a simplified imaging system. *Appl Opt*. 2022;61:5916–5925.
109. Kubala K, Dowski E, Cathey WT. Reducing complexity in computational imaging systems. *Opt Express*. 2003;11:2102–2108.
110. Luo Y, Zhao Y, Li J, Çetintaş E, Rivenson Y, Jarrahi M, Ozcan A. Computational imaging without a computer: Seeing through random diffusers at the speed of light. *eLight*. 2022;2:4.
111. Cossairt OS, Gupta M, Nayar SK. When does computational imaging improve performance? *IEEE Trans Image Process*. 2013;22:447–458.
112. Sidorenko P, Lahav O, Cohen O. Ptychographic ultrahigh-speed imaging. *Opt Express*. 2017;25:10997–11008.
113. Mochizuki F, Kagawa K, Okihara SI, Seo MW, Zhang B, Takasawa T, Yasutomi K, Kawahito S. Single-event transient imaging with an ultra-high-speed temporally compressive

multi-aperture CMOS image sensor. *Opt Express*. 2016;24(4):4155–4176.
114. Matlis NH, Axley A, Leemans WP. Single-shot ultrafast tomographic imaging by spectral multiplexing. *Nat Commun*. 2012;3:1111.
115. Fienup JR. Phase retrieval algorithms: A comparison. *Appl Opt*. 1982;21:2758–2769.
116. Miao J, Charalambous P, Kirz J, Sayre D. Extending the methodology of X-ray crystal-lography to allow imaging of micrometre-sized non-crystalline specimens. *Nature*. 1999;400:342–344.
117. Wengrowicz O, Peleg O, Loevsky B, Chen BK, Haham GI, Sainadh US, Cohen O. Experimental time-resolved imaging by multiplexed ptychography. *Opt Express*. 2019;27:24568.
118. Rodenburg JM. Ptychography and related diffractive imaging methods. *Adv Imaging Electron Phys*. 2008;150:87–184.
119. Rodenburg JM, Faulkner HML. A phase retrieval algorithm for shifting illumination. *Appl Phys Lett*. 2004;85(20): 4795–4797.
120. Batey DJ, Claus D, Rodenburg JM. Information multiplexing in ptychography. *Ultramicroscopy*. 2014;138:13–21.
121. Thibault P, Menzel A. Reconstructing state mixtures from diffraction measurements. *Nature*. 2013;494(7435):68–71.
122. Gerchberg R, Saxton W. A practical algorithm for the determination of phase from image and diffraction plane pictures. *Optik*. 1972;35:227–246.
123. Abbey B. From grain boundaries to single defects: A review of coherent methods for materials imaging in the x-ray sciences. *JOM*. 2013;65:1183–1201.
124. Pan X, Liu C, Zhu J. Single-shot ptychographical iterative engine based on multi-beam illumination. *Appl Phys Lett*. 2013;103:171105.
125. Sidorenko P, Cohen O. Single-shot ptychography. *Optica*. 2016;3(1):9.
126. Li P, Edo T, Batey D, Rodenburg J, Maiden A. Breaking ambiguities in mixed state ptychography. *Opt Express*. 2016;24:9038–9052.
127. Zhang F, Chen B, Morrison GR, Vila-Comamala J, GuizarSicairos M, Robinson IK. Phase retrieval by coherent modulation imaging. *Nat Commun*. 2016;7:13367.
128. Fienup JR. Reconstruction of an object from the modulus of its Fourier transform. *Opt Lett*. 1978;3:27–29.
129. Donoho DL. Compressed sensing. *IEEE T Inform Theory*. 2006;52(4):289–1306.
130. Yin F, Meng YZ, Yang Q, Kai L, Liu Y, Hou X, Lu Y, Chen F. High precision reconstruction for compressed femtosecond dynamics images based on the TVAL3 algorithm. *Opt. Mater. Express*. 2022;12(11):4435–4443.
131. Jin C, Qi D, Yao J, He Y, Ding P, Guo Z, Huang Z, He Y, Yao Y, Wang Z, et al. Weighted multi-scale denoising via adaptive multi-channel fusion for compressed ultrafast photography. *Opt Express*. 2022;30:31157–31170.
132. Haocheng T, Ting M, Xianglei L, Yaodan H, Jingqin S, Yanlei Z, Ping L, Jinyang L, Downer MC, Zhengyan L. Single-shot compressed optical field topography. *Light Sci Appl*. 2022;11:244.
133. Sansone G, Benedetti E, Calegari F, Vozzi C, Avaldi L, Flammini R, Poletto L, Villoresi P, Altucci C, Velotta R, et al. Isolated single-cycle attosecond pulses. *Science*. 2006;314:443.
134. Herman GT. *Fundamentals of computerized tomography: Image reconstruction from projections*. 2nd ed. London: Springer; 2009.
135. Gaumnitz T, Jain A, Pertot Y, Huppert M, Jordan I, Ardana-Lamas F, Wörner HJ. Streaking of 43-attosecond soft-x-ray pulses generated by a passively CEP-stable mid-infrared driver. *Opt Express*. 2017;25(22):27506–27518.
136. Feist A, Rubiano da Silva N, Liang W, Ropers C, Schäfer S. Nanoscale diffractive probing of strain dynamics in ultrafast transmission electron microscopy. *Struct Dyn*. 2018;5:014302.
137. Geohegan DB, Puretzky AA, Duscher G, Pennycook SJ. Time-resolved imaging of gas phase nanoparticle synthesis by laser ablation. *Appl Phys Lett*. 1998;72:2987.
138. Kim T, Liang J, Zhu L, Wang LV. Picosecond-resolution phase-sensitive imaging of transparent objects in a single shot. *Sci Adv*. 2020;6:eaay6200.
139. Zeng X, Wang C, Cai Y, Lin Q, Lu X, Lin J, Yuan X, Cao W, Ai Y, Xu S. High spatial-resolution biological tissue imaging in the second near-infrared region via optical parametric amplification pumped by an ultrafast vortex pulse. *Chin Opt Lett*. 2022;20(10):100003.
140. Qiu X, Li F, Zhang W, Zhu Z, Chen L. Spiral phase contrast imaging in nonlinear optics: Seeing phase objects using invisible illumination. *Optica*. 2018;5(2):208–212.
141. Liu SK, Yang C, Liu SL, Zhou ZY, Li Y, Li YH, Xu ZH, Guo GC, Shi BS. Up-conversion imaging processing with field-of-view and edge enhancement. *Phys Rev Appl*. 2019;11:044013.
142. Liang J, Wang P, Zhu L, Wang LV. Single-shot stereo-polarimetric compressed ultrafast photography for light-speed observation of high-dimensional optical transients with picosecond resolution. *Nat Commun*. 2020;11(1):5252.
143. Chong TC, Hong MH, Shi LP. Laser precision engineering: From microfabrication to nanoprocessing. *Laser Photonics Rev*. 2010;4:123–143.
144. Sugioka K. Hybrid femtosecond laser three-dimensional micro- and nanoprocessing: A review. *Int J Extrem Manuf*. 2019;1(1):Article 012003.
145. Chen H, He X, Qing L, Wu Y, Ren C, Sheriff RE, Zhu C. Real-world single image super-resolution: A brief review. *Inform Fusion*. 2022;79:124–145.
146. Li X, Cao G, Zhang Y, Shafique A, Fu P. Combining synthesis sparse with analysis sparse for single image super-resolution. *Signal Process Image Commun*. 2020;83:Article 115805.
147. Zhang K, Wang Z, Li J, Gao X, Xiong Z. Learning recurrent residual regressors for single image super-resolution. *Signal Process*. 2019;154:324–337.
148. Tang MW, Liu XW, Wen Z, Lin F, Meng C, Liu X, Ma Y, Yang Q. Far-field superresolution imaging via spatial frequency modulation. *Laser Photonics Rev*. 2020;14(11):1900011.
149. Hao X, Kuang C, Li Y, Liu X. Evanescent-wave-induced frequency shift for optical superresolution imaging. *Opt Lett*. 2013;38:2455–2458.
150. Lai Y, Xue Y, Côté CY, Liu X, Laramée A, Jaouen N, Légaré F, Tian L, Liang J. Single-shot ultraviolet compressed ultrafast photography. *Laser Photonics Rev*. 2020;14(10):2000122.
151. Ding P, Yao Y, Qi D, Yang C, Cao F, He Y, Yao J, Jin C, Huang Z, Deng L, et al. Single-shot spectral-volumetric compressed ultrafast photography. *Adv Photon*. 2021;3(4):Article 045001.
152. Li J, Lu J, Chew A, Han S, Li J, Wu Y, Wang H, Ghimire S, Chang Z. Attosecond science based on high harmonic generation from gases and solids. *Nat Commun*. 2020;11:Article 2748.
153. Yang Y, Mainz RE, Rossi GM, Scheiba F, Silva-Toledo MA, Keathley PD, Cirmi G, Kärtner FX. Strong-field coherent

control of isolated attosecond pulse generation. *Nat Commun*. 2021;12:Article 6641.
154. Pushkin A, Migal E, Suleimanova D, Mareev E, Potemkin F. High-power solid-state near- and Mid-IR ultrafast laser sources for strong-field science. *Photo-Dermatology*. 2022;9(2):90.
155. Dhillon S. Mid-infrared ultrashort pulse generation. *Nat Photon*. 2021;15:869–870.
156. Liao G-Q, Liu H, Scott GG, Zhang Y-H, Zhu B-J, Zhang Z, Li Y-T, Armstrong C, Zemaityte E, Bradford P, et al. Towards terawatt-scale spectrally tunable terahertz pulses via relativistic laser-foil interactions. *Phys Rev X*. 2020;10(3):Article 031062.
157. Fülöp JA, Tzortzakis S, Kampfrath T. Laser-driven strong-field terahertz sources. *Adv Optical Mater*. 2020;8(3):1900681.
158. Haenlein M, Kaplan A. A brief history of artificial intelligence: On the past, present, and future of artificial intelligence. *Calif Manag Rev*. 2019;61(4):5–14.
159. Ma YY, Feng XH, Gao L. Deep-learning-based image reconstruction for compressed ultrafast photography. *Opt Lett*. 2020;45(16):4400–4403.
160. Yang C, Yao Y, Jin C, Qi D, Cao F, He Y, Yao J, Ding P, Gao L, Jia T, et al. High-fidelity image reconstruction for compressed ultrafast photography via an augmented-Lagrangian and deep-learning hybrid algorithm. *Photon. Res*. 2021;9(2):B30–B37.
161. Luo XG. Subwavelength artificial structures: Opening a new era for engineering optics. *Adv Mater*. 2019;31(4):1804680.
162. Divitt S, Zhu W, Zhang C, Lezec H, Agrawal A. Ultrafast optical pulse shaping using dielectric metasurfaces. *Science*. 2019;364(6443):890–894.
163. Hu HM, Ji BY, Song HB, Lang P, Lin JQ. Ultrafast spatiotemporal control of the femtosecond Bessel surface plasmon polariton by a chirped laser pulse. *Optics Commun*. 2023;526:Article 128910.
164. Makwana M, Craster R, Guenneau S. Topological beam-splitting in photonic crystals. *Opt Express*. 2019;27(11):16088–16102.
165. Chang H, Chang Q, Xi J, Hou T, Su R, Ma P, Wu J, Li C, Jiang M, et al. First experimental demonstration of coherent beam combining of more than 100 beams. *Photon Res*. 2020;8(12):1943–1948.